Growth factor receptor binding protein 14 inhibition triggers insulin-induced mouse hepatocyte proliferation and is associated with hepatocellular carcinoma

Lucille Morzyglod, Michèle Caüzac, Lucie Popineau, Pierre-Damien Denechaud, Lluis Fajas, Bruno Ragazzon, Véronique Fauveau, Julien Planchais, Mireille Vasseur-Cognet, Laetitia Fartoux, et al.

Grb14 inhibition triggers insulin-induced mouse hepatocyte proliferation and is associated with hepatocellular carcinoma

Lucille Morzyglod[1,2,3], Michèle Caüzac[1,2,3], Lucie Popineau[1,2,3], Pierre-Damien Denechaud[4,5], Luis Fajas[4,5], Bruno Ragazzon[1,2,3], Véronique Fauveau[1,2,3], Julien Planchais[1,2,3], Mireille Vasseur-Cognet[6,7,8], Laetitia Fartoux[9,10], Olivier Scatton[10,11], Olivier Rosmorduc[9,10], Sandra Guilmeau[1,2,3], Catherine Postic[1,2,3], Chantal Desdouets[1,2,3], Christèle Desbois-Mouthon[7], Anne-Françoise Burnol[1,2,3] *

[1] Inserm, U1016, Institut Cochin, Paris, France

[2] CNRS, UMR8104, Paris, France

[3] Université Paris Descartes, Sorbonne Paris Cité, France

[4] Department of Physiology, University of Lausanne, Lausanne CH-1015, Switzerland

[5] Center for Integrative Genomics, University of Lausanne, Lausanne CH-1015, Switzerland

[6] UMR IRD 242, UPEC, CNRS 7618, UPMC 113, INRA 1392, Paris7 113, Institut d'Ecologie et des Sciences de l'Environnement de Paris, 93140 Bondy, France

[7] Sorbonne Universités, Paris, France

[8] Institut National de la Santé et de la Recherche Médicale, Paris, France

[9] APHP, Hôpital La Pitié Salpêtrière, Service d'Hépato-Gastroentérologie, F-75013 Paris, France

[10] Sorbonne Universités, UPMC Univ Paris 06, INSERM, Centre de Recherche Saint-Antoine (CRSA), F-75012 Paris, France

[11] APHP, Hôpital La Pitié-Salpêtrière, Service de Chirurgie Hépatobiliaire et Transplantation, F-75013 Paris, France

This article has been accepted for publication and undergone full peer review but has not been through the copyediting, typesetting, pagination and proofreading process which may lead to differences between this version and the Version of Record. Please cite this article as doi: 10.1002/hep.28972

Keywords : S6K; E2F1 ; insulin signaling ; IR-A/IR-B ; adenoviral shRNA

Contact information :

Dr. Anne-Francoise Burnol

tel. : +33153732709, fax : +33144412421, E-mail : anne-francoise.burnol@inserm.fr

The authors have no conflict of interest.

List of abbreviations

BrdU : bromodeoxyuridin ; DKO : double S6K knockout ; EGF : epidermal growth factor ; Grb14 : Growth factor receptor binding protein 14 ; GSEA : gene set enrichment analysis ; HCC : hepatocellular carcinoma ; iLIRKO : inducible liver insulin receptor knockout ; IR : insulin receptor ; mTORC1 : mechanistic target of rapamycin complex 1 ; PCNA : proliferating cell nuclear antigen ; PI3K : phosphatidylinositol-3 kinase ; Rb : retinoblastoma.

Financial supports

This work was supported by grants from the Agence nationale de la recherche (ANR-06-Grb14, ANR-10-Wnt-Metaboliv, ANR-09-JCJC-0057) and by the Fondation pour la Recherche Médicale (Labélisation Equipe). The work performed within the Saint-Antoine Research Center was supported by grants from the Institut National du Cancer (INCa-DGOS_5790) and the Ligue contre le Cancer (Comité de Paris). LM and LP were supported by a PhD grant from the French Ministry of Research, and LP had a fellowship from the Fondation pour la Recherche Médicale.

Abstract

Metabolic diseases such as obesity and type 2 diabetes are recognized as independent risk factors for hepatocellular carcinoma (HCC). Hyperinsulinemia, a hallmark of these pathologies, is suspected to be involved in HCC development. The molecular adapter Grb14 is an inhibitor of insulin receptor (IR) catalytic activity, highly expressed in the liver. To study its involvement in hepatocyte proliferation we specifically inhibited its liver expression using an shRNA strategy in mice. Enhanced insulin signaling upon *Grb14* downregulation (Grb14i) was accompanied by a transient induction of S phase entrance by quiescent hepatocytes, indicating that Grb14 is a potent repressor of cell division. The proliferation of Grb14-deficient hepatocytes was cell autonomous, as it was also observed in primary cell cultures. Combined *Grb14* downregulation and insulin signaling blockade using pharmacological approaches as well as genetic mouse models demonstrated that Grb14i-mediated hepatocyte division involved IR activation and was mediated by the mTORC1-S6K pathway and the transcription factor E2F1. In order to determine a potential dysregulation in *GRB14* gene expression in human pathophysiology, a collection of 85 human HCC was investigated. This revealed a highly significant and frequent decrease in *GRB14* expression in hepatic tumors when compared to adjacent nontumoral parenchyma, 60% of the tumors exhibiting reduced Grb14 mRNA level. Conclusion : our study establishes Grb14 as a physiological repressor of insulin mitogenic action in the liver, and further supports that dysregulation of insulin signaling is associated with HCC.

Insulin is a unique hormone controlling metabolic homeostasis. Secreted by the pancreatic beta cells in response to increased circulating blood glucose levels, insulin acts on its metabolic target tissues to maintain glucose and lipid metabolic homeostasis (1). In addition to its metabolic actions, insulin behaves as a growth factor stimulating cell proliferation in many cell types. However, a direct effect of insulin on cell proliferation is poorly documented *in vivo*, although its involvement is increasingly suspected in the development of cancer (2). Epidemiological studies highlighted that individuals with obesity or type 2 diabetes are at higher risk of developing and dying from multiple cancers, including hepatocellular carcinoma (HCC). Among the factors that are susceptible to link obesity, diabetes and cancer, hyperinsulinemia, which develops secondary to insulin resistance, is a likely candidate (3, 4). Furthermore, the expression of the insulin receptor (IR) is deregulated in several types of human tumors, suggesting that IR signaling is involved in the tumorigenic process (5, 6). IR exists as two splicing isoforms : IR-B which is mainly expressed in tissues involved in the metabolic effects of insulin, and IR-A which is expressed in fetal cells and in many tumor cells and is considered to be more mitogenic than IR-B (7). Interestingly, we recently showed an overexpression of IR-A to the detriment of IR-B in human HCC, suggesting that IR can be directly implicated in liver neoplastic transformation and/or tumor growth and progression (6).

Insulin stimulation of the IR activates two main intracellular signaling pathways, the PI3-kinase (PI3K)-Akt and the Ras-ERK1/2 pathways. Metabolic actions of insulin are predominantly mediated by the PI3K-Akt signaling cascade, and the mitogenic effect is classically considered to be triggered by the Ras-ERK1/2 pathway (8, 9). However, depending on the cell type, PI3K-Akt and Ras-ERK1/2 signaling pathways are likely to be involved to variable degrees (10, 11). While the molecular pathways mediating insulin-induced metabolic actions are well characterized, the mechanisms whereby insulin stimulates mitogenesis and regulates cell cycle and G1/S progression remain to be fully clarified (12, 13). Insulin signaling and action are also tightly monitored by negative

regulators, including the molecular adapter Grb14 (9, 14). We previously reported that Grb14, which is highly expressed in the liver, is an inhibitor of IR catalytic activity, and that its downregulation improves IR signaling and hepatic glucose production in cultured hepatocytes (15-18). However, *Grb14* deletion also enhances insulin-induced cell growth in mouse embryonic fibroblasts, suggesting that both mitogenic and metabolic effects of insulin are controlled by Grb14 expression level (19).

In this study we demonstrate that Grb14 expression is required to protect hepatocytes against an insulin-dependent mitogenic signal. We unravel that downstream the IR-B hepatocyte proliferation is driven by Akt-mTORC1 signaling and the Rb/E2F1 pathway. Furthermore, we show that *GRB14* expression is significantly decreased in human HCC, hence providing a molecular link to support a role for insulin signaling in the development of HCC.

EXPERIMENTAL PROCEDURES

Animals and treatments

Nine-week-old male mice were purchased from Harlan Laboratories (C57BL6/J) and adapted to the environment for one week before study. The iLIRKO (inducible liver IR knockout) mice were described previously (20). Fifteen-week-old male mice were studied three weeks after IR deletion. Generation of S6K1$^{-/-}$/S6K2$^{-/-}$ mice has been previously described (21). E2F1 KO mice were from Jackson laboratories. All mice were housed in colony cages with a 12-h light/dark cycle in a temperature-controlled environment and had free access to water and regular diet (65% carbohydrate, 11% fat and 24% protein). All procedures were carried out according to the French guidelines for the care and use of experimental animals and were approved by the "Direction départementale des services vétérinaires de Paris". Mice were anesthetized with isoflurane before the injection through the penis vein with 2.10^9 pfu of recombinant adenovirus expressing either a control shRNA (USi) or a shRNA targeting *Grb14* (Grb14i) (18) in a final volume of 150 µl sterile physiological serum. For experiments with inhibitors, mice were injected intraperitoneally twice (18 hours and 2 hours) before sacrifice either with Akt inhibitor VIII (Akti, 50 mg/kg, Sigma Aldrich) or Rapamycin (4.5 mg/kg, Invivogen). Mice were sacrificed two days after adenoviral injection, and two hours prior to sacrifice they were intraperitoneally injected with 50 mg/kg of BrdU (Sigma). Blood was collected, part of liver tissue was fixed in 4% neutral buffered formalin for immunohistochemistry analysis. The remaining liver tissue was flash-frozen in liquid nitrogen and stored at –80 °C until used.

Patients and liver tissue specimens

Eighty-five HCC (T) and paired adjacent non-tumour (NT) liver tissues were collected from patients undergoing curative liver resection for HCC at the Saint-Antoine Hospital and stored in a tumour biobank (Pathology department, Saint-Antoine hospital) in accordance with the French laws and regulations (CNIL number 1913901 v0). Part of this tissue

collection (43 paired T/NT) has been used in our previous study where it was designed as collection #2 (6). Clinicopathologic characteristics of the 85 patients are recapitulated in Supplementary Table S2.

Experiments in primary hepatocytes, hepatoma cell lines, protein and mRNA analysis, immunohistochemistry, transcriptome preparation and data analysis are described in the Supplementary material.

RESULTS

Liver specific down-regulation of Grb14 expression induces hepatocyte proliferation

To experimentally investigate the consequences of an acute depletion of Grb14 on hepatocyte proliferation, we downregulated *Grb14* expression in liver of C57Bl/6 mice using an adenoviral strategy. Mice were injected with either Grb14 adenoviral shRNA (Grb14i) or control RNA (USi) and livers were analyzed after 48h. Grb14 liver expression was decreased by 40% and 30% at the mRNA and protein levels respectively in Grb14i-treated mice (Fig.1A-B). This significantly improved insulin signaling, as shown by the enhanced phosphorylation of ERK1/2 and Akt and of the downstream effectors of the Akt pathway (GSK3β, S6K, 4EBP1) (Fig.1B, Supporting Figure S1A). A liver transcriptomic analysis was performed and Gene set enrichment analysis (GSEA) showed a robust positive association between genes altered by *Grb14* downregulation and both cell cycle and DNA replication pathways (Fig.1C) especially with the KEGG cell cycle gene set (Fig.1D). Activation of genes involved in cellular proliferation is thus the prominent feature after a decrease in Grb14 liver content.

To validate the transcriptomic data on the proliferation state of liver cells, mice were injected with BrdU two hours before the sacrifice. As shown in Fig.1E, 48h after the Grb14i injection, 33% of the hepatocytes were in the S phase of the cell cycle, as compared to 2% in control USi animals. *In situ* BrdU staining was mainly detected in hepatocytes, and very few other cell types were labelled. Accordingly, several cyclins (E (*ccne*), A (*ccna2*) and B1 (*ccnb1*)) which control the progression of the cell cycle, and markers of proliferation (PCNA) or mitosis (phospho-histone H3 and *Ki67*) were strikingly increased at mRNA level and/or protein level after *Grb14* downregulation (Fig.1F). By contrast, cyclin D1 (*ccnd1*) was only moderately increased (Fig.1F). Hepatocyte division induced by *Grb14* downregulation was transiently peaking two days after adenoviral infection (Supporting Fig.S1B). From day four, BrdU labelling was similar in USi and Grb14i mice liver, while concomitantly Grb14 protein

expression continued to decrease from day 2 to day 4 (Supporting Fig.S1B-C). Apoptosis was not modified by Grb14i treatment as assessed by TUNEL immunolabelling (Supporting Fig.S1D), and this short term inhibition of *Grb14* expression did not induce liver toxicity as shown by ALAT and ASAT circulating concentrations (Supporting Fig.S1E).

The effect of Grb14 inhibition on hepatocyte proliferation was further investigated *in vitro* in primary mouse hepatocytes. Hepatocytes isolated from C57Bl/6 mice were treated with USi or Grb14i together with a mitogenic cocktail including insulin that induced one cell division and progression through S phase 48h after plating (22). After Grb14i infection, Grb14 protein expression was inhibited by about 30% after 24h of culture and by more than 90% from 36h and until the end of the experiment at 60h (Fig.2B). *Ki67* expression was significantly enhanced in Grb14i- compared to USi-treated cells from 24h to 48h, indicating that the mitogenic signal was strengthened in the absence of Grb14 (Fig.2A). Similarly, the expression of cyclin E (*ccne*), cyclin A (*ccna2*) and cyclin B1 (*ccnb1*) was significantly enhanced by *Grb14* downregulation, throughout the length of the experiment (Fig.2B-C). By contrast, cyclin D1 (*ccnd1*) mRNA levels were not altered by Grb14i treatment.

Altogether these results reveal that Grb14 acts as a potent inhibitor of hepatocyte division, acting in a cell autonomous manner probably at the G1/S transition.

Hepatocyte proliferation induced by Grb14 downregulation requires its molecular partner, the insulin receptor

In liver, IR-B is the major isoform expressed, in agreement with the metabolic function of insulin in this organ (Supporting Fig.S2). Upon *Grb14* downregulation IR-B expression was slightly decreased by 20% while IR-A expression was not induced. IR-B thus remained the major isoform expressed in Grb14i liver (Supporting Fig.S2). To investigate whether the proliferative effect observed after liver *Grb14* inhibition was attributable to IR activation or to other Grb14 partners, we used an inducible liver specific IR knock-out mouse line (iLIRKO)

(20) (Fig.3A). Basal mRNA and protein Grb14 levels were lower in iLIRKO livers compared to control, according to the previously reported stimulatory effect of insulin on *Grb14* expression (23) (Fig.3B). The increase in BrdU incorporation in hepatocytes nuclei observed in control $IR^{lox/lox}$ mice injected with Grb14i was markedly decreased by the deletion of the IR (Fig.3C). Phosphorylation of ERK1/2, Akt and S6K was strikingly reduced in liver from iLIRKO mice treated with USI or with Grb14i. This provides evidence that insulin signaling pathways were severely blunted by IR knockout and were not activated by Grb14i treatment, while p-4EBP1 was still detected in iLIRKO mice and increased after *Grb14* downregulation (Fig.3D). The effect of *Grb14* downregulation on *Ki67* expression and on the expression of cyclin E (*ccne1)*, cyclin A (*ccna2*) and cyclin B1 (*ccnb1*) was inhibited in liver from iLIRKO compared to $IR^{lox/lox}$ mice (Fig.3D-E). These data indicate that hepatocyte proliferation induced by *Grb14* downregulation was at least partly attributable to the activation of IR signaling, suggesting then that insulin can act as a powerful mitogen in the liver.

Hepatocyte division induced by Grb14 silencing is mediated by the PI3K-Akt-mTORC1 signaling pathway

To evaluate the contribution of the PI3K-Akt-mTORC1 pathway in Grb14i-induced hepatocyte division, we first used a pharmacological approach. Inhibition of PI3K by wortmannin, of Akt by AktiVIII (Akti) or of mTORC1 by rapamycin significantly reduced the increase in BrdU hepatocyte staining induced by the downregulation of *Grb14* (Fig.4A and data not shown). In correlation with BrdU labelling, Grb14i-mediated increased expression of cyclin A (*ccna2*), cyclin B1 (*ccnb1*) and *Ki67* was severely inhibited by Akti and rapamycin, while cyclin E (*ccne1)* was not significantly altered (Fig.4B-C). To further investigate the role of mTORC1, we then used S6K DKO mice, which are deleted for both *S6k1* and *S6k2* genes (21). While as expected S6K expression was totally inhibited in S6K DKO mice liver, Akt and 4EBP1 signaling pathways were preserved (Fig.5C). S6K gene deletion reduced the

induction of BrdU hepatocyte nuclear incorporation after the Grb14i treatment (Fig.5A-B). The increase in *Ki67* expression and cyclin A (*ccna2*) and cyclin B1 (*ccnb1*) gene and protein expression caused by *Grb14* downregulation was also significantly inhibited in S6K DKO liver, while cyclin E (*ccne1)* mRNA expression was not modified (Fig.5C-D). Altogether, these data suggest that hepatocyte proliferation in Grb14i liver is mediated by the Akt-S6K pathway.

Functional Rb/E2F1 pathway is crucial for hepatocyte division induced by Grb14 downregulation

The next step was to identify the pathway downstream of mTORC1/S6K which mediates Grb14i-dependent hepatocyte division. We analyzed the expression and phosphorylation status of the retinoblastoma protein (Rb), a well characterized transcription co-repressor which controls the G1 restriction point. Unphosphorylated Rb binds to the E2F transcription factors, repressing their activity, but the complex is disrupted after Rb phosphorylation, allowing E2F to induce cyclin gene expression and cell cycle progression (24). The phosphorylation of Rb on different serine residues was strikingly increased by Grb14i treatment in mouse liver as well as in primary hepatocytes, and Rb protein level was also enhanced (Fig.6A-B). The transcriptional activity of E2F factors was investigated using a E2F-RE reporter gene in transfected primary hepatocytes. Stimulation of hepatocytes by the mitogenic treatment induced E2F activity, and *Grb14* downregulation further enhanced this activity (Fig.6C). GSEA showed a significant enrichment in Grb14i liver for genes upregulated or downregulated by the deletion of the three members of the Rb family (Rb TKO) (25) (Fig.6D), supporting an activation of the Rb-E2F pathway upon *Grb14* downregulation. Interestingly, the increase in Rb phosphorylation and E2F1 mRNA and protein expression induced by the downregulation of *Grb14* were reduced by Akti or rapamycin treatment, suggesting that the Akt-mTORC1 pathway was involved in Rb-E2F1

activation in Grb14i mice (Fig.6E). This was further illustrated by the decreased effect of *Grb14* downregulation on liver *e2f1* expression in iLIRKO mice (Fig.6F) and on Rb phosphorylation in S6K DKO mice (supporting Fig.S3A). We finally validated these results by investigating the effect of Grb14i in E2F1 KO mice. The induction of hepatocyte proliferation consecutive to *Grb14* downregulation was strongly reduced in E2F1 KO mice, as revealed by BrdU immuno-labelling (Fig.7A-B, Supporting Fig.S3B). As expected, the downregulation of *Grb14* stimulated phosphorylation of ERK1/2, Akt and S6K similarly in E2F1 KO and WT mice liver (Fig.7C), indicating that the absence of E2F1 expression did not modify upstream insulin signaling. In contrast, the increase in cyclin A and B1 protein expression, and in *Ki67, ccne*, *ccna2* and *ccnb1* mRNA expression induced by *Grb14* downregulation was inhibited in E2F1 KO mice liver (Fig.7C-D). Altogether, these results strongly suggest that the IR-dependent proliferative effect induced by *Grb14* downregulation is mediated at least in part by the Rb-E2F1 pathway.

In basal conditions, insulin binding to its hepatic IR promotes the regulation of glucose and lipid metabolic homeostasis through the activation of the Akt-mTORC1 pathway (1). However, these data suggest that the release of the endogenous repressive action of Grb14 on the IR stimulates a proliferative insulin signal mediated by Akt-mTORC1 and the Rb-E2F1 complex (Fig.7E).

Grb14 expression is decreased in human hepatoma cell lines and HCC

To investigate whether dysregulation of Grb14 expression could be related to human hepatocyte transformation, we first compared *GRB14* mRNA level between freshly isolated hepatocytes and five hepatoma cell lines. Interestingly, *GRB14* expression was significantly decreased from 50% to 95% in hepatoma cells compared to normal hepatocytes (Fig.8A). In addition, whereas *E2F1* was hardly detectable in primary hepatocytes, its expression was strikingly enhanced in all hepatoma cell lines. Interestingly, forced expression of *Grb14* in

PLC/PRF5, HepG2 or Huh6 cells, which expressed low endogenous levels of the gene, significantly reduced insulin-induced proliferation (Fig.8B), arguing that Grb14 opposes insulin proliferative action in hepatoma cells.

We then examined *GRB14* expression level in a collection of 85 HCC and paired adjacent nontumoral parenchyma. Sixty percent of tumors exhibited a significant decreased expression of *GRB14* (mean=58%, p=0.0004), while *E2F1* expression was enhanced in 89% of HCC (mean=3160%, p<0.0001) (Fig.8C-D). We also investigated data sets in Oncomine and showed that *GRB14* expression was significantly decreased in HCC compared to adjacent parenchyma in Roessler liver and Roessler liver 2 collections, including respectively 22 and 225 HCC samples (Supporting Fig.S4). Of note, a significant association was observed between low *GRB14* expression and poor differentiation state in our HCC collection (Supporting Table S3). Furthermore, in accordance with our previous study (6), IR-A expression and the IR-A/IR-B ratio were significantly increased in this HCC collection (Supporting Fig.S5). The decrease in *GRB14* and increase in IR-A expression in HCC is supportive of a potential proliferative role of insulin in these tumors.

DISCUSSION

This work reveals that an acute inhibition of *Grb14* expression in mouse liver is sufficient to trigger hepatocyte proliferation, an effect mostly dependent on IR expression and downstream signaling. We further unveil that Grb14i liver mitogenic action is mediated by mTORC1/S6K and involves the activation of the E2F1 transcription factor. Our study also demonstrates that *GRB14* expression is decreased in 60% of the human HCC specimens tested. The occurrence of *GRB14* downregulation together with IR-A induction in HCC supports an increased mitogenic activity of insulin during HCC development. Overall, this report thus identifies insulin as a potent mitogenic factor on hepatocytes and highlights *GRB14* as a gatekeeper of insulin proliferative signal, which dysregulation could be involved in the pathogenic development of HCC.

Grb14 downregulation was sufficient to activate the insulin signaling pathways and sett off a surge in cell cycle entry in hepatocytes. The release of this proliferative effect in iLIRKO mice pointed to the IR as a key actor in this phenomenon, and unraveled an unsuspected insulin mitogenic potency in mouse liver. Interestingly, this effect was likely mediated by IR-B isoform, the major isoform expressed in the liver, since the expression of IR-A was not increased upon *Grb14* inhibition. Moreover, our study clearly identified the mTORC1-S6K pathway as the driver of insulin-induced hepatocyte proliferation. Dysregulation of the mTOR signaling pathway is common in multiple cancers, and has been associated with both cell growth, through the activation of protein and lipid synthesis, and cell proliferation (26). Downstream mTORC1 aberrant activation, either S6K or 4EBP1 can mediate cell proliferation and tumorigenesis depending on the cellular context (27, 28). mTOR and S6K were found activated in 40-50% of human HCC, playing a pivotal role in the pathogenesis of HCC and associated with a poor prognosis (29, 30). Hepatocytes are quiescent cells that can enter into the cell cycle to regenerate the liver mass after partial hepatectomy. It has been shown that S6K plays a special role in this particular situation, as it

is required for cyclin D1 expression and hepatocyte proliferation (31). In addition, liver regeneration is inhibited by rapamycin through decrease S6K activation without modification of 4EBP1 phosphorylation (32). In accordance with these studies, our data support a potent proliferative function of the mTORC1-S6K pathway downstream IR signaling. The transient window where hepatocytes were allowed to cycle (cell division was triggered at day 2 while *Grb14* was only partly inhibited) suggests that powerfull counterregulatory mechanisms were operating to suppress the proliferative signal, as observed in liver regeneration after partial hepatectomy (33).

Insulin is a prominent growth factor, but its molecular targets regulating the cell cycle are still poorly defined (13). The Rb-E2F1 complex plays a pivotal role in cell cycle progression. Phosphorylation of Rb by cyclin-dependent kinases results in Rb inhibition and in the activation of E2F transcription factors to allow cells to enter S phase (34). Here we show that hepatocyte proliferation consecutive to the downregulation of *Grb14* was mediated by Rb phosphorylation and E2F1 activation in an IR-dependent manner. Many mitogens stimulate cell division by regulating this pathway, but this is, to our knowledge, the first study to point E2F1 as a mediator of insulin-induced cell proliferation. Overexpression of liver E2F1 in transgenic mice or inactivation of the Rb proteins results in liver dysplasia and hepatocarcinogenesis, indicating that E2F1 can contribute to liver oncogenesis by promoting cell proliferation (25, 35). Interestingly, E2F1 expression is enhanced in liver from obese, glucose-intolerant humans and in cirrhotic livers, and is considered as a potential marker for liver fibrosis and both NASH and alcoholic cirrhosis (36, 37). E2F1 is also overexpressed in human HCC and its expression correlates with tumor cell apoptosis (this study, 38). This apparent paradoxical observation can be explained by the dual function of E2F1, which exerts both oncogenic and tumor-suppressive properties (34). This double role was nicely illustrated in transgenic mice overexpressing liver E2F1, E2F1 being pro-proliferative in early stages and pro-apoptotic in latter stages of liver carcinogenesis (35). E2F1 therefore arises

as an important regulator of liver integrity and pathophysiological evolution of chronic liver diseases.

Insulin signaling pathways were similarly activated by *Grb14* downregulation or by feeding. The question then arises of the molecular mechanism that triggers cell division when IR signaling is stimulated by the release of the repressive action of Grb14 but not after a meal. A first hypothesis is provided by the induction of Grb14 expression under insulin stimulation, as shown here in primary hepatocytes and previously reported in adipocytes (23). The increase in Grb14 generated by this feed-back loop can tightly regulate the length of signaling and, consequently, the mitogenic effect of insulin. An alternative is that Grb14 binding partners mediate additional proliferative signals. Interestingly, we recently showed that Grb14 and the ubiquitin ligase Chfr (Checkpoint with forkhead and Ring Finger domains) cooperate in a negative feed-back loop controlling insulin-induced cell proliferation in *Xenopus* oocytes (39). Chfr is a tumor-suppressor gene, whose promoter is hypermethylated in numerous cancers (40). Of note, Chfr methylation correlates with the progression of HCC and is proposed to play a role in the pathogenesis of this cancer (41, 42). Grb14 also forms in the liver a constitutive complex with the adapter p62/sqstm1, which controls the timely transit of cells through mitosis and tumor cell proliferation (43-45). Cell cycle progression could then be altered by the release of p62 consecutive to *Grb14* silencing. Most studies were focused on the metabolic role of Grb14 and very few informations are currently available on the mitogenic function of Grb14 or *Grb14* expression in cancer (14). *GRB14* regulates cell cycle progression in breast cancer cells in an insulin-dependent manner (46), and a high expression of *GRB14* is an independent good prognosis factor for breast cancer patients (47). Our present data support an anti-proliferative function of Grb14 downstream of insulin signaling, and show that low level of *GRB14* could be a *bona fide* marker of HCC. However, the molecular mechanisms involved in the decreased *GRB14* expression in HCC remain to be clarified.

Among the molecular mechanisms potentially underlying the link between metabolic diseases and the increased risk of cancer, the insulin axis deserves a particular interest (2). Metabolic diseases are characterized by insulin resistance and elevated levels of circulating insulin. Of note, in the liver some pathways are resistant to the action of insulin, such as gluconeogenesis, while others remain exquisitely sensitive to the hormone, such as lipogenesis and, possibly, cell proliferation. There is to date no evidence for an implication of insulin/IR in cellular transformation and tumor initiation, but our study provides evidence that hyperinsulinemia can be instrumental for cell proliferation in liver, and offer an attractive molecular explanation for the link between hyperinsulinemia and increased HCC prevalence.

ACKNOWLEDGMENTS

The authors would like to thank Florent Dumont and Franck Letourneur from the Plateform Genom'ic (Institut Cochin, Inserm U1016, Paris) for microarray experiments and analysis, Isabelle Lagoutte and the staff of the Cochin's animal facility, the Cochin HistIM Facility (Institut Cochin, Inserm U1016, Paris) for performing liver sections, the Plateforme of Biochemistry from the Institut Claude Bernard, Paris, for plasma analysis. The authors acknowledge the « Tumeur Est » from the Groupe Hospitalier HUEP of AP-HP for access to HCC samples, Yves Chrétien for statistical analysis, Dominique Wendum for histopathology analyses, Mario Pende and Ganna Panzyuk for kindly provinding S6K DKO mice. Christine Perret and Hélène Gilgenkrantz are gratefully acknowledged for helpful discussions and critical reading of the manuscript. Mice used in this study were housed in an animal facility equipped with the help of the Région Ile de France. The work was performed within the Département Hospitalo-Universitaire (DHU) AUToimmune and HORmonal diseasesS.

REFERENCES

1. Saltiel AR, Kahn CR. Insulin signalling and the regulation of glucose and lipid metabolism. Nature 2001;414:799-806.

2. Gallagher EJ, LeRoith D. The proliferating role of insulin and insulin-like growth factors in cancer. Trends Endocrinol Metab 2010;21:610-618.

3. Gallagher EJ, LeRoith D. Obesity and Diabetes: The Increased Risk of Cancer and Cancer-Related Mortality. Physiol Rev 2015;95:727-748.

4. Chettouh H, Lequoy M, Fartoux L, Vigouroux C, Desbois-Mouthon C. Hyperinsulinaemia and insulin signalling in the pathogenesis and the clinical course of hepatocellular carcinoma. Liver Int 2015;35:2203-2217.

5. Cox ME, Gleave ME, Zakikhani M, Bell RH, Piura E, Vickers E, Cunningham M, et al. Insulin receptor expression by human prostate cancers. Prostate 2009;69:33-40.

6. Chettouh H, Fartoux L, Aoudjehane L, Wendum D, Claperon A, Chretien Y, Rey C, et al. Mitogenic insulin receptor-A is overexpressed in human hepatocellular carcinoma due to EGFR-mediated dysregulation of RNA splicing factors. Cancer Res 2013;73:3974-3986.

7. Belfiore A, Frasca F, Pandini G, Sciacca L, Vigneri R. Insulin receptor isoforms and insulin receptor/insulin-like growth factor receptor hybrids in physiology and disease. Endocr Rev 2009;30:586-623.

8. Jensen M, Palsgaard J, Borup R, de Meyts P, Schaffer L. Activation of the insulin receptor (IR) by insulin and a synthetic peptide has different effects on gene expression in IR-transfected L6 myoblasts. Biochem J 2008;412:435-445.

9. Boucher J, Kleinridders A, Kahn CR. Insulin receptor signaling in normal and insulin-resistant states. Cold Spring Harb Perspect Biol 2014;6.

10. Svegliati-Baroni G, Ridolfi F, Di Sario A, Casini A, Marucci L, Gaggiotti G, Orlandoni P, et al. Insulin and insulin-like growth factor-1 stimulate proliferation and type I collagen accumulation by human hepatic stellate cells: differential effects on signal transduction

pathways. Hepatology 1999;29:1743-1751.

11. Conejo R, Lorenzo M. Insulin signaling leading to proliferation, survival, and membrane ruffling in C2C12 myoblasts. J Cell Physiol 2001;187:96-108.

12. Wu MY, Cully M, Andersen D, Leevers SJ. Insulin delays the progression of Drosophila cells through G2/M by activating the dTOR/dRaptor complex. Embo J 2007;26:371-379.

13. Svendsen AM, Winge SB, Zimmermann M, Lindvig AB, Warzecha CB, Sajid W, Horne MC, et al. Down-regulation of cyclin G2 by insulin, IGF-I (insulin-like growth factor 1) and X10 (AspB10 insulin): role in mitogenesis. Biochem J 2014;457:69-77.

14. Desbuquois B, Carre N, Burnol AF. Regulation of insulin and type 1 insulin-like growth factor signaling and action by the Grb10/14 and SH2B1/B2 adaptor proteins. Febs J 2013;280:794-816.

15. Kasus-Jacobi A, Perdereau D, Auzan C, Clauser E, Van Obberghen E, Mauvais-Jarvis F, Girard J, et al. Identification of the rat adapter Grb14 as an inhibitor of insulin actions. J. Biol. Chem. 1998;273:26026-26035.

16. Bereziat V, Kasus-Jacobi A, Perdereau D, Cariou B, Girard J, Burnol AF-. Inhibition of insulin receptor catalytic activity by the molecular adapter Grb14. J Biol Chem 2002;277:4845-4852.

17. Desbuquois B, Bereziat V, Authier F, Girard J, Burnol AF. Compartmentalization and in vivo insulin-induced translocation of the insulin-signaling inhibitor Grb14 in rat liver. Febs J 2008;275:4363-4377.

18. Carré N, Caüzac M, Girard J, Burnol A-F. Dual effect of the adapter Grb14 on insulin action in primary hepatocytes. Endocrinology 2008;149:3109-3117.

19. Goenaga D, Hampe C, Carré N, Cailliau K, Browaeys-Poly E, Perdereau D, Holt LJ, et al. Molecular determinants of Grb14-mediated inhibition of insulin signaling. Mol Endocrinol 2009;23:1043-1051.

20. Nemazanyy I, Montagnac G, Russell RC, Morzyglod L, Burnol AF, Guan KL, Pende M,

et al. Class III PI3K regulates organismal glucose homeostasis by providing negative feedback on hepatic insulin signalling. Nat Commun 2015;6:8283.

21. Pende M, Um SH, Mieulet V, Sticker M, Goss VL, Mestan J, Mueller M, et al. S6K1(-/-)/S6K2(-/-) mice exhibit perinatal lethality and rapamycin-sensitive 5'-terminal oligopyrimidine mRNA translation and reveal a mitogen-activated protein kinase-dependent S6 kinase pathway. Mol Cell Biol 2004;24:3112-3124.

22. Guidotti JE, Bregerie O, Robert A, Debey P, Brechot C, Desdouets C. Liver cell polyploidization: a pivotal role for binuclear hepatocytes. J Biol Chem 2003;278:19095-19101.

23. Cariou B, Capitaine N, Le Marcis V, Vega N, Bereziat V, Kergoat M, Laville M, et al. Increased adipose tissue expression of Grb14 in several models of insulin resistance. Faseb J 2004;18:965-967.

24. Burkhart DL, Sage J. Cellular mechanisms of tumour suppression by the retinoblastoma gene. Nat Rev Cancer 2008;8:671-682.

25. Viatour P, Ehmer U, Saddic LA, Dorrell C, Andersen JB, Lin C, Zmoos AF, et al. Notch signaling inhibits hepatocellular carcinoma following inactivation of the RB pathway. J Exp Med 2011;208:1963-1976.

26. Laplante M, Sabatini DM. mTOR signaling in growth control and disease. Cell 2012;149:274-293.

27. Alliouachene S, Tuttle RL, Boumard S, Lapointe T, Berissi S, Germain S, Jaubert F, et al. Constitutively active Akt1 expression in mouse pancreas requires S6 kinase 1 for insulinoma formation. J Clin Invest 2008;118:3629-3638.

28. Hsieh AC, Costa M, Zollo O, Davis C, Feldman ME, Testa JR, Meyuhas O, et al. Genetic dissection of the oncogenic mTOR pathway reveals druggable addiction to translational control via 4EBP-eIF4E. Cancer Cell 2010;17:249-261.

29. Sahin F, Kannangai R, Adegbola O, Wang J, Su G, Torbenson M. mTOR and P70 S6

kinase expression in primary liver neoplasms. Clin Cancer Res 2004;10:8421-8425.

30. Zhou L, Huang Y, Li J, Wang Z. The mTOR pathway is associated with the poor prognosis of human hepatocellular carcinoma. Med Oncol 2010;27:255-261.

31. Espeillac C, Mitchell C, Celton-Morizur S, Chauvin C, Koka V, Gillet C, Albrecht JH, et al. S6 kinase 1 is required for rapamycin-sensitive liver proliferation after mouse hepatectomy. J Clin Invest 2011;121:2821-2832.

32. Jiang YP, Ballou LM, Lin RZ. Rapamycin-insensitive regulation of 4e-BP1 in regenerating rat liver. J Biol Chem 2001;276:10943-10951.

33. Michalopoulos GK. Liver regeneration. J Cell Physiol 2007;213:286-300.

34. Polager S, Ginsberg D. E2F - at the crossroads of life and death. Trends Cell Biol 2008;18:528-535.

35. Conner EA, Lemmer ER, Omori M, Wirth PJ, Factor VM, Thorgeirsson SS. Dual functions of E2F-1 in a transgenic mouse model of liver carcinogenesis. Oncogene 2000;19:5054-5062.

36. Zhang Y, Xu N, Xu J, Kong B, Copple B, Guo GL, Wang L. E2F1 is a novel fibrogenic gene that regulates cholestatic liver fibrosis through the Egr-1/SHP/EID1 network. Hepatology 2014;60:919-930.

37. Denechaud P, Lopez-Mejia I, Giralt Coll A, Lai Q, Blanchet E, Delacuisine B, Nicolay B, et al. E2F1 mediates sustained lipogenesis and contributes to hepatic steatosis. J. Clin. Invest 2015;126:137-150.

38. Palaiologou M, Koskinas J, Karanikolas M, Fatourou E, Tiniakos DG. E2F-1 is overexpressed and pro-apoptotic in human hepatocellular carcinoma. Virchows Arch 2012;460:439-446.

39. Perdereau D, Cailliau K, Browaeys-Poly E, Lescuyer A, Carré N, Benhamed F, Goenaga D, et al. Insulin-induced cell division is controlled by the adaptor Grb14 in a Chfr-dependent manner. Cell Signal 2015;27:798-806.

40. Derks S, Cleven AH, Melotte V, Smits KM, Brandes JC, Azad N, van Criekinge W, et al. Emerging evidence for CHFR as a cancer biomarker: from tumor biology to precision medicine. Cancer Metastasis Rev 2014;33:161-171.

41. Sakai M, Hibi K, Kanazumi N, Nomoto S, Inoue S, Takeda S, Nakao A. Aberrant methylation of the CHFR gene in advanced hepatocellular carcinoma. Hepatogastroenterology 2005;52:1854-1857.

42. Li Z, Zhang H, Yang J, Hao T, Li S. Promoter hypermethylation of DNA damage response genes in hepatocellular carcinoma. Cell Biol Int 2012;36:427-432.

43. Cariou B, Perdereau D, Cailliau K, Browaeys-Poly E, Béréziat V, Vasseur-Cognet M, Girard J, et al. The adapter protein ZIP binds Grb14 and regulates its inhibitory action on insulin signaling by recruiting Protein Kinase Cz. Mol Cell Biol 2002;22:6959-6970.

44. **Popineau L, Morzyglod L**, Carré N, Cauzac M, Bossard P, Prip-Buus C, Lenoir V, et al. Novel Grb14-Mediated Cross Talk between Insulin and p62/Nrf2 Pathways Regulates Liver Lipogenesis and Selective Insulin Resistance. Mol Cell Biol 2016;36:2168-2181.

45. Linares JF, Amanchy R, Greis K, Diaz-Meco MT, Moscat J. Phosphorylation of p62 by cdk1 controls the timely transit of cells through mitosis and tumor cell proliferation. Mol Cell Biol 2011;31:105-117.

46. Kairouz R, Parmar J, Lyons RJ, Swarbrick A, Musgrove EA, Daly RJ. Hormonal regulation of the Grb14 signal modulator and its role in cell cycle progression of MCF-7 human breast cancer cells. J Cell Physiol 2005;203:85-93.

47. Huang O, Jiang M, Zhang X, Xie Z, Chen X, Wu J, Liu H, et al. Grb14 as an independent good prognosis factor for breast cancer patients treated with neoadjuvant chemotherapy. Jpn J Clin Oncol 2013;43:1064-1072.

48. Subramanian A, Tamayo P, Mootha VK, Mukherjee S, Ebert BL, Gillette MA, Paulovich A, et al. Gene set enrichment analysis: a knowledge-based approach for interpreting genome-wide expression profiles. Proc Natl Acad Sci U S A 2005;102:15545-15550.

FIGURE LEGENDS

Figure 1 : Liver-specific inhibition of *Grb14* improves insulin signaling and induces hepatocyte proliferation in mice. C57Bl/6J mice were intravenously injected with adenovirus expressing unspecific (USi) or Grb14 (Grb14i) shRNA and livers were harvested after two days. (A) qRT-PCR analysis of *Grb14* expression (left part) and quantification of Grb14 protein expression (right part). (B) Western blot analysis of Grb14 expression and intracellular signaling pathways in liver lysates from USi and Grb14i mice. (C) Gene set enrichment analysis (GSEA) (48) were performed with trancriptomic data from C57Bl/6 mice injected with USi (n=3) or Grb14i (n=3) (GEO GSE81387) and with BioCarta and KEGG gene sets. All results are shown in the Supporting Table S1 and here only the best enrichments are shown (FDR q value < 0.001). NES, Normalized Enrichment Score. (D) GSEA plot for the top enriched pathway showing a significant enrichment for genes up-regulated in liver from Grb14i mice with the KEGG list of cell cycle genes. (E) BrdU immunohistochemistry of liver sections (x20) and quantification of BrdU positive cells. (F) Western blot (left) and qRT-PCR (right) analysis of cell cycle markers. Western blots in B and F are from the same experiments (with the same GAPDH loading control) and are shown in two panels for clarity of presentation. Results are the mean ± SEM (n = 6 per group). *p<0.05, **p<0.01 for Grb14i compared to USi mice. mRNA levels are expressed relative to 18S. For Western blot analysis, three representative samples (from six) are shown and GAPDH is used as loading control.

Figure 2 : *Grb14* down-regulation enhances cell division *in vitro* in primary mouse hepatocytes submitted to a mitotic challenge. Primary hepatocytes were infected with USi or Grb14i adenovirus after plating (t=0h) and stimulated with the mitogenic mix. (A) qRT-PCR analysis of *Ki67* expression. (B) Western blot analysis of Grb14 and cyclins expression. (C) qRT-PCR analysis of cyclins expression. Results are the mean ± SEM of three independent

cultures. *p<0.05, **p<0.01, ***p<0.005 for Grb14i compared to USi hepatocytes. mRNA levels are expressed relative to 18S.

Figure 3 : Grb14i-induced hepatocyte proliferation is mediated by the IR. iLIRKO and littermate $IR^{lox/lox}$ control mice were injected with tamoxifen to delete liver IR three weeks before the infection with USi or Grb14i adenovirus. Livers were harvested after two days of infection. (A) qRT-PCR analysis of IR expression. (B) qRT-PCR and quantification of Western blot analysis of *Grb14* expression. (C) BrdU immunohistochemistry of liver sections (x20) and quantification of BrdU positive cells. (D) Western blot analysis of insulin signaling pathways activation and cyclins expression. (E) qRT-PCR analysis of *Ki67* and cyclins expression. Results are the mean ± SEM (n = 8 to 10 per group). *p<0.05, **p<0.01, ***p<0.005 for Grb14i compared to USi mice. $^{\#}$p<0.05, $^{\#\#}$p<0.01, $^{\#\#\#}$p<0.005 for iLIRKO compared to $IR^{lox/lox}$ mice. mRNA levels are expressed relative to 18S. For Western blot analysis, two representative samples from 8-10 per group are shown and GAPDH is used as loading control.

Figure 4 : Hepatocyte division upon *Grb14* downregulation is mediated by the Akt/mTORC1 pathway. C57Bl/6J mice were infected with USi or Grb14i adenovirus and injected intraperitoneally with the indicated inhibitors or the control DMSO (Akti VIII : 50mg/kg, rapamycin : 4.5mg/kg). (A) BrdU immunohistochemistry of liver sections (x20) and quantification of BrdU positive cells. (B) Western blot analysis of Grb14 expression, insulin signaling pathways and cyclins expression. Samples were analyzed on the same blots and the black line indicates cropping of the original blots. (C) qRT-PCR analysis of *Ki67* and cyclins expression. Results are the mean ± SEM (n = 5-6 per group). *p<0.05, **p<0.01, ***p<0.005 for Grb14i compared to USi mice. $^{\#}$p<0.05, $^{\#\#}$p<0.01, $^{\#\#\#}$p<0.005 for inhibitor-compared to DMSO-treated Grb14i mice. mRNA levels are expressed relative to 18S. For Western blot analysis, representative blots of two samples from 5-6 per group are shown and GAPDH is used as loading control.

Figure 5 : S6K is involved in Grb14i-induced hepatocyte proliferation. S6K DKO and WT control mice were injected with USi or Grb14i adenovirus and livers were harvested and analyzed after two days. (A) BrdU immunohistochemistry of liver sections (x20) and quantification of BrdU positive cells. (B) qRT-PCR and quantification of Western blot analysis of Grb14 expression. (C) Western blot analysis of insulin signaling pathways and cyclins expression. (D) qRT-PCR analysis of *Ki67* and cyclins expression. Results are the mean ± SEM (n = 3 to 4 per group). *p<0.05, **p<0.01, ***p<0.005 for Grb14i compared to USi mice. $^{\#}$p<0.05, $^{\#\#}$p<0.01, $^{\#\#\#}$p<0.005 for S6K DKO compared to WT Grb14i mice. mRNA levels are expressed relative to 18S. For Western blot analysis, two representative samples from 3-4 per group are shown and GAPDH is used as loading control.

Figure 6 : Hepatocyte proliferation induced by liver *Grb14* downregulation is mediated by the Rb/E2F1 pathway. (A) Western blot analysis of Rb expression and phosphorylation in liver from USi and Grb14i mice and (B) in primary cultured hepatocytes treated with USi or Grb14i. Blots in (B) are from the same experiment shown in Fig.2B (with the same GAPDH loading control). (C) Activity of an E2F-RE luciferase gene reporter transfected in primary mouse hepatocytes treated with USi or Grb14i. Results are the mean ± SEM of three independent experiments performed in triplicates. (D) Gene set enrichment analysis (GSEA) showed a significant enrichment of genes up and downregulated by liver invalidation of the three Rb genes in mice (GEO GSE19004 (25)) with gene expression profile induced in liver from Grb14i mice. NES, Normalized Enrichment Score. (E) Western blot analysis of Rb expression and phosphorylation and of E2F1 expression (upper part) and qRT-PCR analysis of E2F1 expression (lower part) in liver from USi and Grb14i mice treated with control DMSO, Akti or rapamycin as indicated. (F) E2F1 mRNA expression measured by qRT-PCR in $IR^{lox/lox}$ and iLIRKO mice injected with USi or Grb14i adenovirus.

Figure 7 : Grb14i-induced hepatocyte proliferation is inhibited in E2F1 KO mice. (A) BrdU immunohistochemistry of liver sections (x20) and quantification of BrdU positive cells. (B) qRT-PCR and quantification of Western blot analysis of *Grb14* expression. (C) Western blot analysis of insulin signaling pathways and cyclins expression in liver lysates from E2F1 KO mice and control littermates injected with USi or Grb14i adenovirus. (D) qRT-PCR analysis of *Ki67* and cyclins expression from USi- or Grb14i-mice liver. Results are the mean ± SEM (n = 8 to 13 per group). *p<0.05, **p<0.01, ***p<0.005 for Grb14i compared to USi. $^{\#}$p<0.05, $^{\#\#}$p<0.01, $^{\#\#\#}$p<0.005 for E2F1 KO compared to WT mice. mRNA levels are expressed relative to 18S. For Western blot analysis, two representative samples from 8-13 per group are shown and GAPDH is used as loading control. (E) Model for the regulation of hepatocyte homeostasis through the control by Grb14 of IR signaling. Left part : Grb14 represses IR catalytic activity, contributing to the control of liver metabolic homeostasis. Right part : Grb14 inhibition enhances insulin signaling and promotes a mTORC1-Rb/E2F1 proliferative signal.

Figure 8 : *GRB14* status in human hepatoma cells and HCC tumors. (A) qRT-PCR analysis of *GRB14* (left part) and *E2F1* (right part) expression in normal freshly isolated human hepatocytes (HH) and in hepatoma cell lines. Results are the mean ± SEM (n = 4 per group), * p<0.05 when compared to HH. (B) Cell number after 60h of culture for PLC/PRF5, HepG2 or Huh6 cells transiently transfected with the pcDNA3-Grb14 expression vector or the control empty vector (EV) and cultured in the presence or in the absence of insulin as indicated. Results are the mean ± SEM of three independent experiments, *p<0.05. Upper part : Western blots showing the increased expression of Grb14 in transfected cells. (C-D) qRT-PCR analysis of *GRB14* (C) and *E2F1* (D) mRNA expression in 85 paired HCC (T) and non tumor (NT) adjacent liver tissue samples.

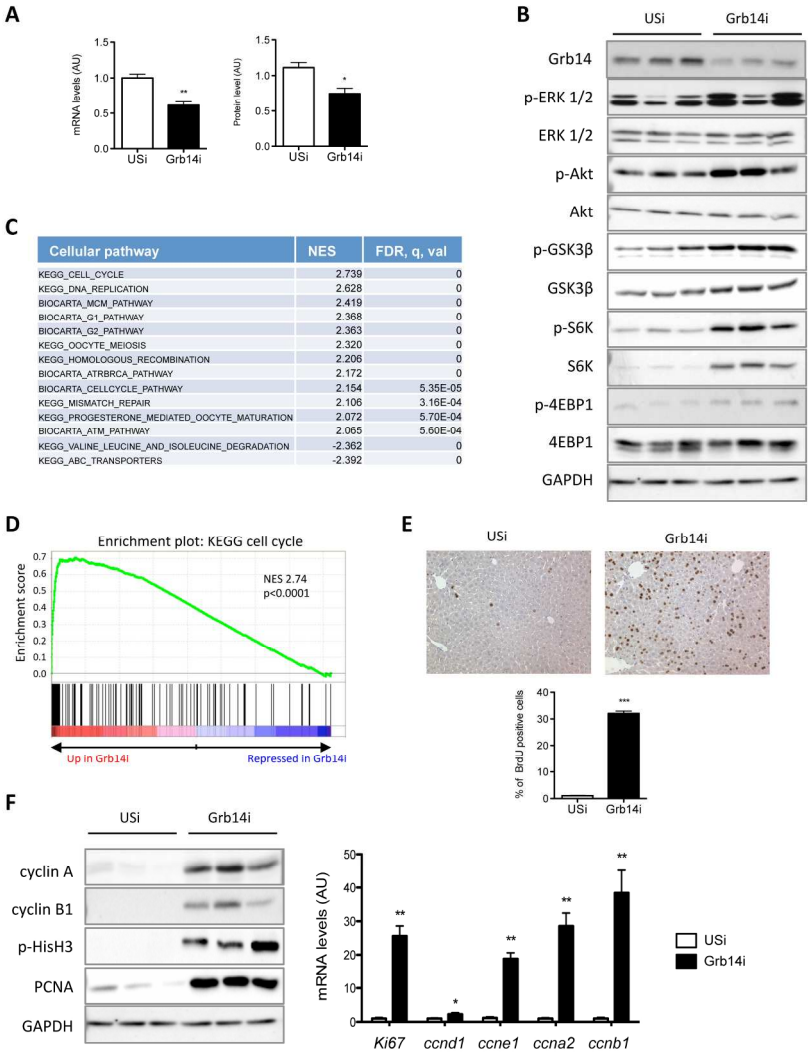

Cellular pathway	NES	FDR, q, val
KEGG_CELL_CYCLE	2.739	0
KEGG_DNA_REPLICATION	2.628	0
BIOCARTA_MCM_PATHWAY	2.419	0
BIOCARTA_G1_PATHWAY	2.368	0
BIOCARTA_G2_PATHWAY	2.363	0
KEGG_OOCYTE_MEIOSIS	2.320	0
KEGG_HOMOLOGOUS_RECOMBINATION	2.206	0
BIOCARTA_ATRBRCA_PATHWAY	2.172	0
BIOCARTA_CELLCYCLE_PATHWAY	2.154	5.35E-05
KEGG_MISMATCH_REPAIR	2.106	3.16E-04
KEGG_PROGESTERONE_MEDIATED_OOCYTE_MATURATION	2.072	5.70E-04
BIOCARTA_ATM_PATHWAY	2.065	5.60E-04
KEGG_VALINE_LEUCINE_AND_ISOLEUCINE_DEGRADATION	-2.362	0
KEGG_ABC_TRANSPORTERS	-2.392	0

Figure 1

Figure 1 : Liver-specific inhibition of Grb14 improves insulin signaling and induces hepatocyte proliferation in mice. C57Bl/6J mice were intravenously injected with adenovirus expressing unspecific (USi) or Grb14 (Grb14i) shRNA and livers were harvested after two days. (A) qRT-PCR analysis of Grb14 expression (left part) and quantification of Grb14 protein expression (right part). (B) Western blot analysis of Grb14 expression and intracellular signaling pathways in liver lysates from USi and Grb14i mice. (C) Gene set enrichment analysis (GSEA) (48) were performed with trancriptomic data from C57Bl/6 mice injected with USi (n=3) or Grb14i (n=3) (GEO GSE81387) and with BioCarta and KEGG gene sets. All results are shown in the Supporting Table S1 and here only the best enrichments are shown (FDR q value < 0.001). NES, Normalized Enrichment Score. (D) GSEA plot for the top enriched pathway showing a significant enrichment for genes up-regulated in liver from Grb14i mice with the KEGG list of cell cycle genes. (E) BrdU immunohistochemistry of liver sections (x20) and quantification of BrdU positive cells. (F) Western blot (left) and qRT-PCR (right) analysis of cell cycle markers. Western blots in B and F are from the same experiments (with the same GAPDH loading control) and are shown in two panels for clarity of presentation. Results are

the mean ± SEM (n = 6 per group). *p<0.05, **p<0.01 for Grb14i compared to USi mice. mRNA levels are expressed relative to 18S. For Western blot analysis, three representative samples (from six) are shown and GAPDH is used as loading control.

191x244mm (300 x 300 DPI)

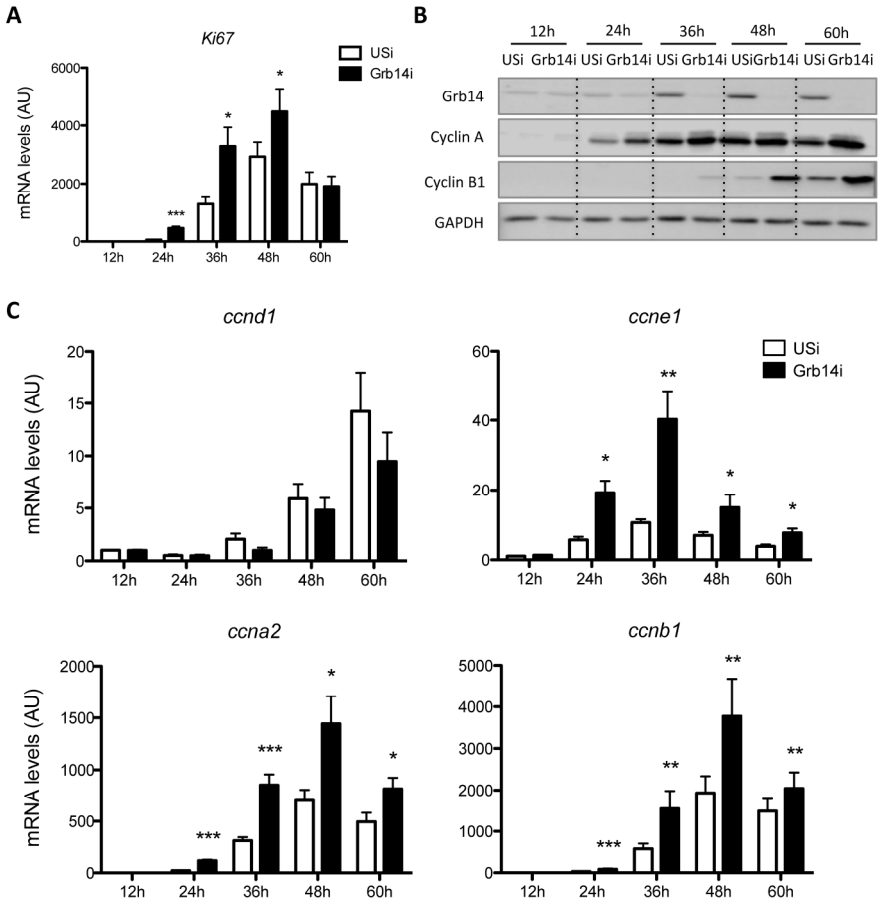

Figure 2

Figure 2 : Grb14 down-regulation enhances cell division in vitro in primary mouse hepatocytes submitted to a mitotic challenge. Primary hepatocytes were infected with USi or Grb14i adenovirus after plating (t=0h) and stimulated with the mitogenic mix. (A) qRT-PCR analysis of Ki67 expression. (B) Western blot analysis of Grb14 and cyclins expression. (C) qRT-PCR analysis of cyclins expression. Results are the mean ± SEM of three independent cultures. *p<0.05, **p<0.01, ***p<0.005 for Grb14i compared to USi hepatocytes. mRNA levels are expressed relative to 18S.

191x212mm (300 x 300 DPI)

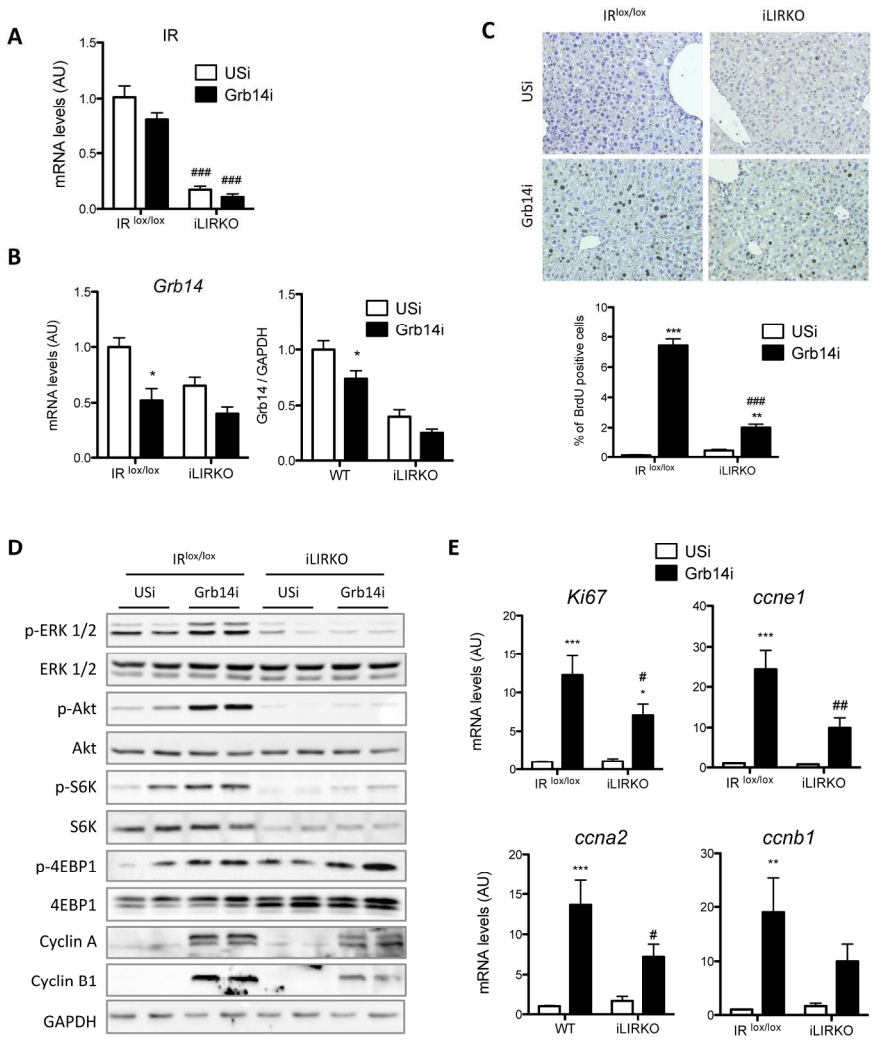

Figure 3

Figure 3 : Grb14i-induced hepatocyte proliferation is mediated by the IR. iLIRKO and littermate IRlox/lox control mice were injected with tamoxifen to delete liver IR three weeks before the infection with USi or Grb14i adenovirus. Livers were harvested after two days of infection. (A) qRT-PCR analysis of IR expression. (B) qRT-PCR and quantification of Western blot analysis of Grb14 expression. (C) BrdU immunohistochemistry of liver sections (x20) and quantification of BrdU positive cells. (D) Western blot analysis of insulin signaling pathways activation and cyclins expression. (E) qRT-PCR analysis of Ki67 and cyclins expression. Results are the mean ± SEM (n = 8 to 10 per group). *p<0.05, **p<0.01, ***p<0.005 for Grb14i compared to USi mice. #p<0.05, ##p<0.01, ###p<0.005 for iLIRKO compared to IRlox/lox mice. mRNA levels are expressed relative to 18S. For Western blot analysis, two representative samples from 8-10 per group are shown and GAPDH is used as loading control.

187x234mm (300 x 300 DPI)

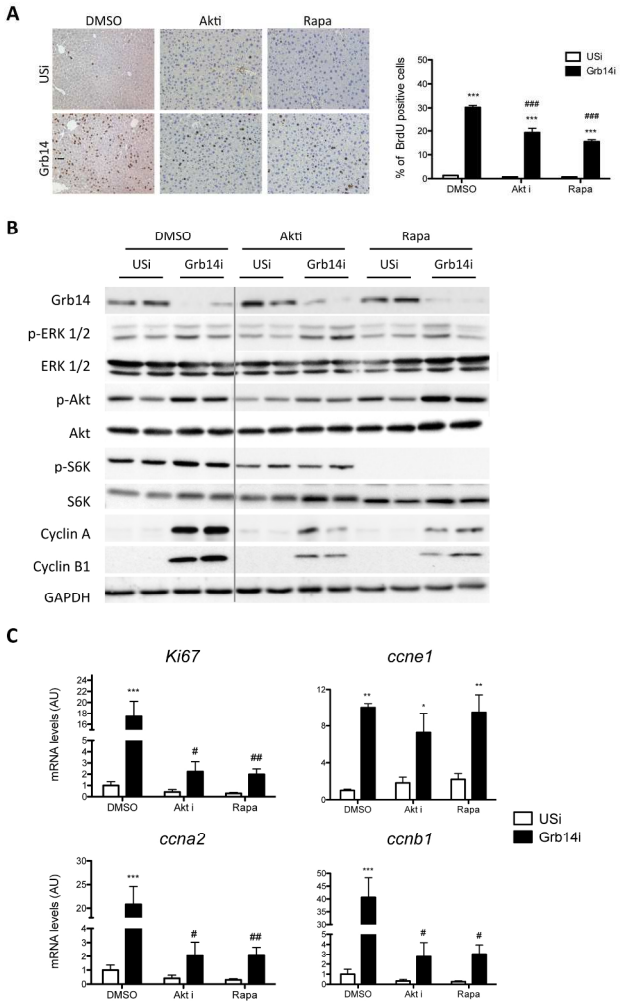

Figure 4

Figure 4

Figure 4 : Hepatocyte division upon Grb14 downregulation is mediated by the Akt/mTORC1 pathway. C57Bl/6J mice were infected with USi or Grb14i adenovirus and injected intraperitoneally with the indicated inhibitors or the control DMSO (Akti VIII : 50mg/kg, rapamycin : 4.5mg/kg). (A) BrdU immunohistochemistry of liver sections (x20) and quantification of BrdU positive cells. (B) Western blot analysis of Grb14 expression, insulin signaling pathways and cyclins expression. Samples were analyzed on the same blots and the black line indicates cropping of the original blots. (C) qRT-PCR analysis of Ki67 and cyclins expression. Results are the mean ± SEM (n = 5-6 per group). *p<0.05, **p<0.01, ***p<0.005 for Grb14i compared to USi mice. #p<0.05, ##p<0.01, ###p<0.005 for inhibitor- compared to DMSO-treated Grb14i mice. mRNA levels are expressed relative to 18S. For Western blot analysis, representative blots of two samples from 5-6 per group are shown and GAPDH is used as loading control.

189x270mm (300 x 300 DPI)

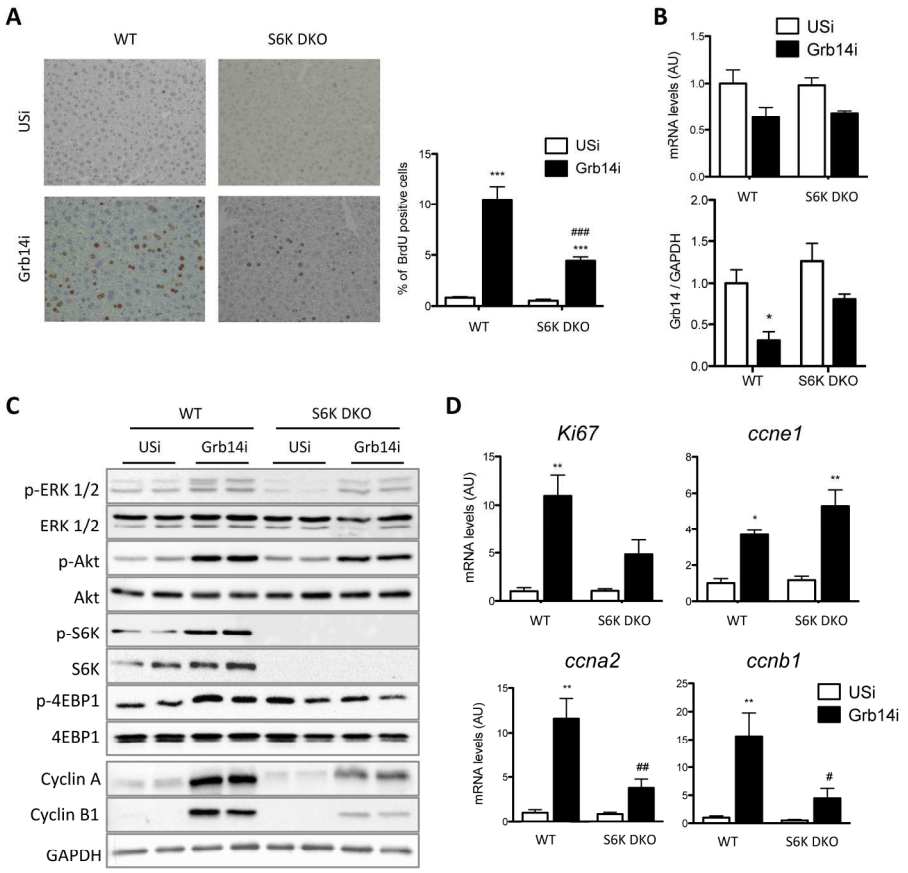

Figure 5

Figure 5 : S6K is involved in Grb14i-induced hepatocyte proliferation. S6K DKO and WT control mice were injected with USi or Grb14i adenovirus and livers were harvested and analyzed after two days. (A) BrdU immunohistochemistry of liver sections (x20) and quantification of BrdU positive cells. (B) qRT-PCR and quantification of Western blot analysis of Grb14 expression. (C) Western blot analysis of insulin signaling pathways and cyclins expression. (D) qRT-PCR analysis of Ki67 and cyclins expression. Results are the mean ± SEM (n = 3 to 4 per group). *p<0.05, **p<0.01, ***p<0.005 for Grb14i compared to USi mice. #p<0.05, ##p<0.01, ###p<0.005 for S6K DKO compared to WT Grb14i mice. mRNA levels are expressed relative to 18S. For Western blot analysis, two representative samples from 3-4 per group are shown and GAPDH is used as loading control.

187x201mm (300 x 300 DPI)

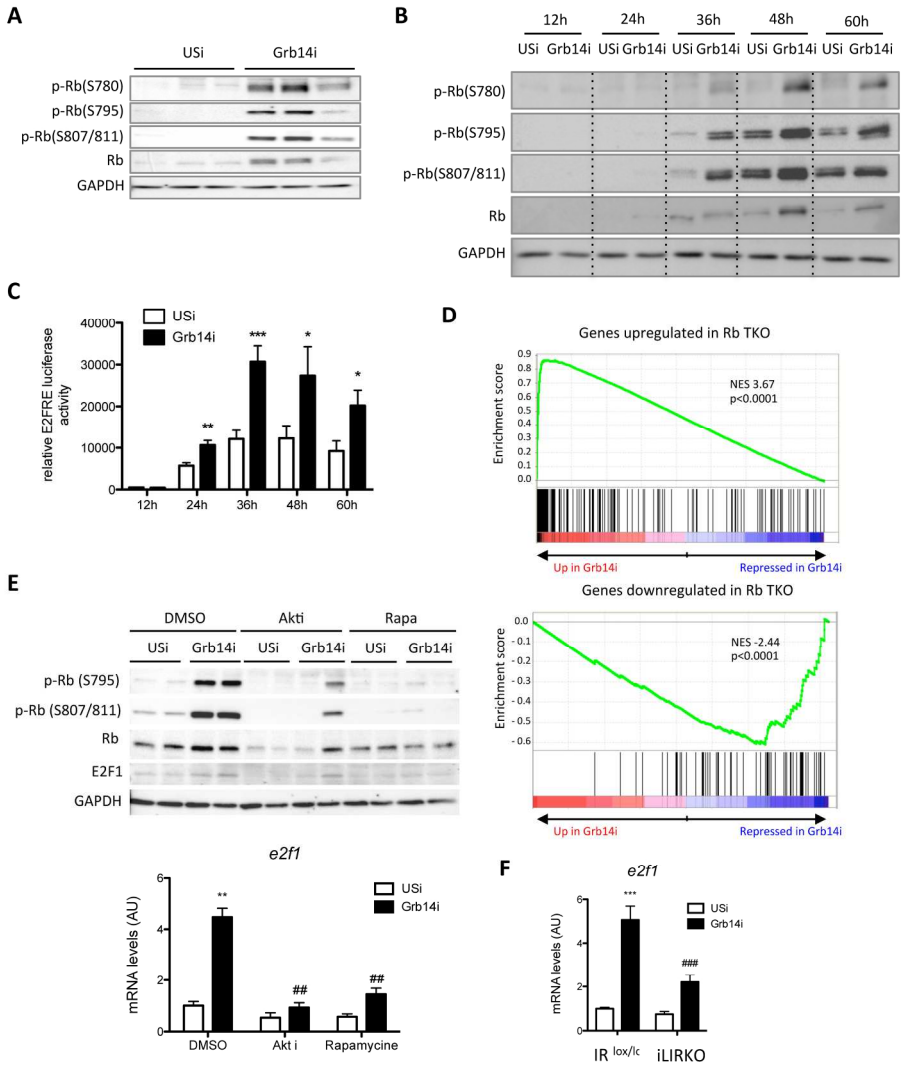

Figure 6

Figure 6 : Hepatocyte proliferation induced by liver Grb14 downregulation is mediated by the Rb/E2F1 pathway. (A) Western blot analysis of Rb expression and phosphorylation in liver from USi and Grb14i mice and (B) in primary cultured hepatocytes treated with USi or Grb14i. Blots in (B) are from the same experiment shown in Fig.2B (with the same GAPDH loading control). (C) Activity of an E2F-RE luciferase gene reporter transfected in primary mouse hepatocytes treated with USi or Grb14i. Results are the mean ± SEM of three independent experiments performed in triplicates. (D) Gene set enrichment analysis (GSEA) showed a significant enrichment of genes up and downregulated by liver invalidation of the three Rb genes in mice (GEO GSE19004 (25)) with gene expression profile induced in liver from Grb14i mice. NES, Normalized Enrichment Score. (E) Western blot analysis of Rb expression and phosphorylation and of E2F1 expression (upper part) and qRT-PCR analysis of E2F1 expression (lower part) in liver from USi and Grb14i mice treated with control DMSO, Akti or rapamycin as indicated. (F) E2F1 mRNA expression measured by qRT-PCR in IRlox/lox and iLIRKO mice injected with USi or Grb14i adenovirus.

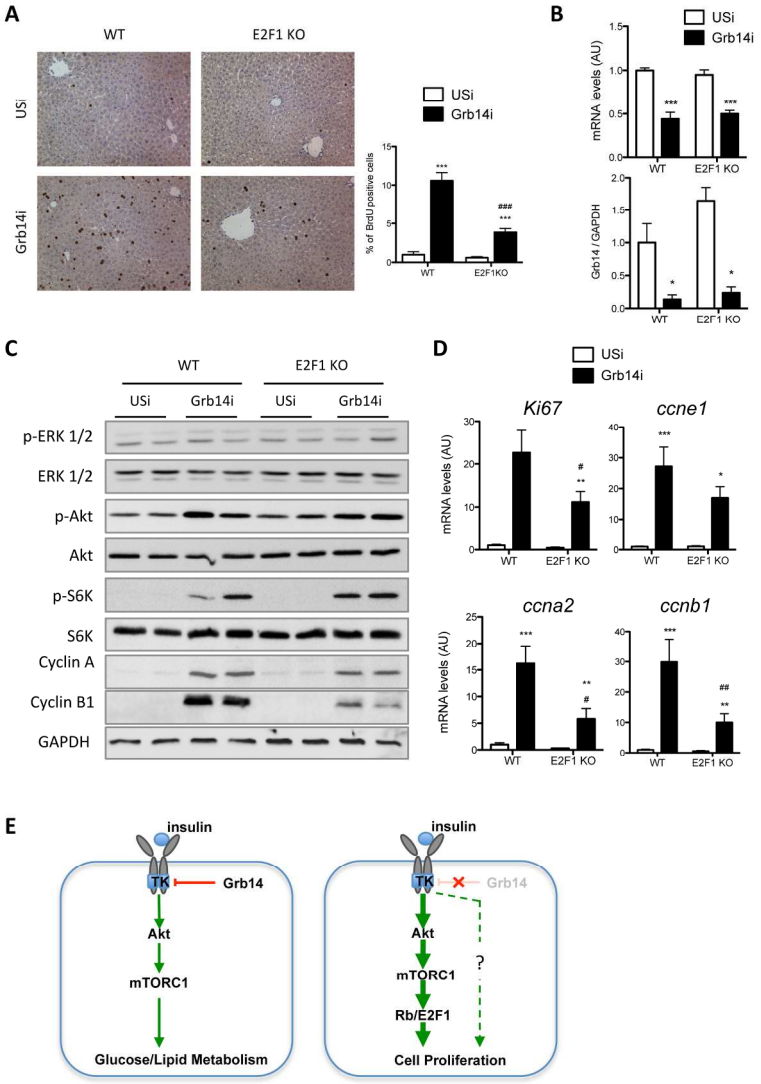

Figure 7

Figure 7 : Grb14i-induced hepatocyte proliferation is inhibited in E2F1 KO mice. (A) BrdU immunohistochemistry of liver sections (x20) and quantification of BrdU positive cells. (B) qRT-PCR and quantification of Western blot analysis of Grb14 expression. (C) Western blot analysis of insulin signaling pathways and cyclins expression in liver lysates from E2F1 KO mice and control littermates injected with USi or Grb14i adenovirus. (D) qRT-PCR analysis of Ki67 and cyclins expression from USi- or Grb14i-mice liver. Results are the mean ± SEM (n = 8 to 13 per group). *p<0.05, **p<0.01, ***p<0.005 for Grb14i compared to USi. #p<0.05, ##p<0.01, ###p<0.005 for E2F1 KO compared to WT mice. mRNA levels are expressed relative to 18S. For Western blot analysis, two representative samples from 8-13 per group are shown and GAPDH is used as loading control. (E) Model for the regulation of hepatocyte homeostasis through the control by Grb14 of IR signaling. Left part : Grb14 represses IR catalytic activity, contributing to the control of liver metabolic homeostasis. Right part : Grb14 inhibition enhances insulin signaling and promotes a mTORC1-Rb/E2F1 proliferative signal.

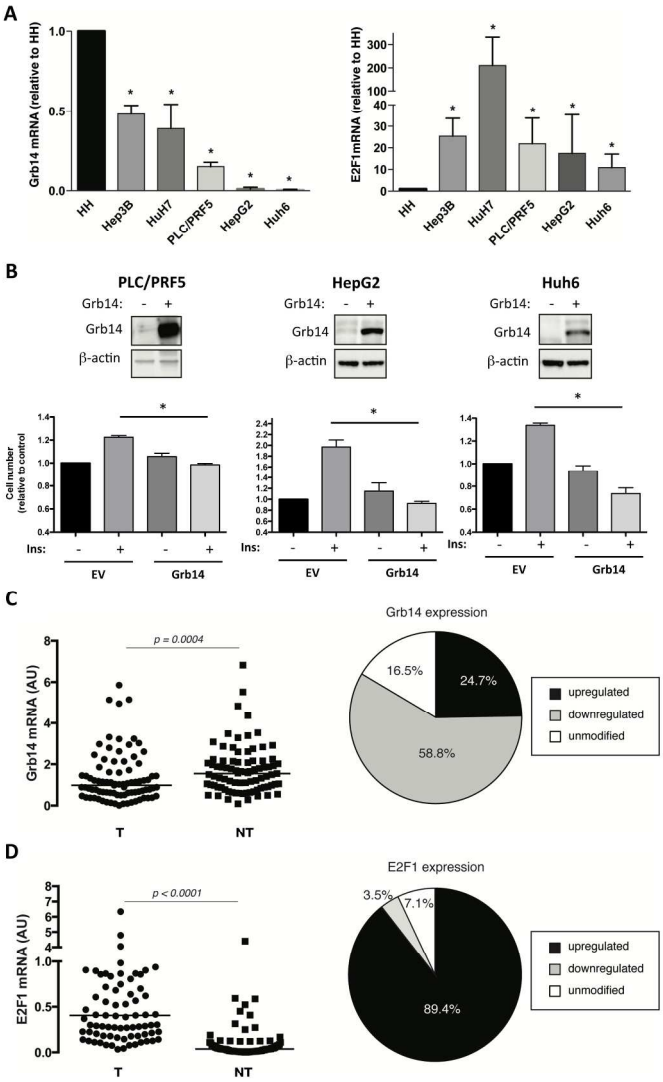

Figure 8

Figure 8 : GRB14 status in human hepatoma cells and HCC tumors. (A) qRT-PCR analysis of GRB14 (left part) and E2F1 (right part) expression in normal freshly isolated human hepatocytes (HH) and in hepatoma cell lines. Results are the mean ± SEM (n = 4 per group), * $p<0.05$ when compared to HH. (B) Cell number after 60h of culture for PLC/PRF5, HepG2 or Huh6 cells transiently transfected with the pcDNA3-Grb14 expression vector or the control empty vector (EV) and cultured in the presence or in the absence of insulin as indicated. Results are the mean ± SEM of three independent experiments, *$p<0.05$. Upper part : Western blots showing the increased expression of Grb14 in transfected cells. (C-D) qRT-PCR analysis of GRB14 (C) and E2F1 (D) mRNA expression in 85 paired HCC (T) and non tumor (NT) adjacent liver tissue samples.

187x259mm (300 x 300 DPI)

Supporting informations

EXPERIMENTAL PROCEDURES

Primary hepatocytes cultures and luciferase reporter assays

Hepatocytes were isolated from livers of fed eight- to ten-week-old male C57BL6/J mice by an *in situ* collagenase method as described previously (1). Four hours after spreading, hepatocytes were incubated with mitogenic factors (EGF 50ng/ml, insulin 0.68mM, sodium pyruvate 0.2mM) and 3 pfu/cell of USi or Grb14i adenovirus. Medium containing the mitogenic factors was freshly replaced at 12h and 36h. Primary cultured hepatocytes were transfected with a 3X E2F1-RE luciferase plasmid (2) using lipofectamine 2000 (LifeTechnologies) according to the manufacturer's instructions. Luciferase activity was measured every 12h from 12 to 60h after reporter transfection.

Primary cultures of human hepatocytes were established as previously described (3).

Hepatoma cells culture and transient transfection experiments

HepG2, Hep3B, and HuH7 cells were obtained from the American Type Culture Collection (ATCC). Huh6 and PLC/PRF5 cells were provided by Dr Christine Perret (Institut Cochin, France). Cell line authentication was routinely performed by using a panel of nine ATCC short tandem repeats. Cell lines were cultured as previously reported (4) and routinely controlled for mycoplasma contamination. Cells seeded in 24-well dishes (3-5x10^4 cells/well) were transfected with 0.5 mg of the pcDNA3 plasmid coding for rat Grb14 (5) or of a control empty pcDNA3 plasmid by using Lipofectamine 3000 (Huh6, PLC/PRF5, Thermo Fisher Scientific) or TransIT-2020 (HepG2, Mirus Bio LLC) according to manufacturers recommendations. Serum-deprived cells were then treated or not with insulin (10^{-8} M) during 60 h and counted using Bio-Rad TC20 cell counter.

Protein extraction and immunoblotting

For whole-cell protein extracts, cultured cells or mouse livers were solubilized at 4°C in a buffer containing Tris-HCl (50mM, pH 7,5), 150mM NaCl, 5mM EDTA, 1% Triton X-100 plus protease inhibitor tablet (Roche) and phosphatases inhibitors (5mM NaF, 2mM sodium orthovanadate and 30mM sodium pyrophosphate). Supernatants were collected after a 15 min centrifugation at 13000 rpm at 4°C. Proteins were quantified using the Bradford method (BioRad Protein Assay). Lysates were subjected to SDS-PAGE electrophoresis and immunoblotted with the indicated antibodies. The immunoreactive bands were revealed using the "Clarity Western ECL Substrate" (BIO-RAD) and the BioRad ChemiDoc MP device. Primary antibodies used were: anti-p-4EBP1(S65), anti-p-Akt(S473), anti-p-ERK1/2(T202/Y204), anti-p-GSK3β (S9), anti-p-p70-S6K(T389), anti-p-Rb(S780), anti-p-Rb(S795), anti-p-Rb(S807/811), anti-4EBP1, anti-Akt, anti-cyclin D1, anti-cyclin B1, anti-ERK, anti-GSK3β, anti-p70-S6K, anti-PCNA, anti-Rb from Cell Signaling Technology; anti-GAPDH, anti-cyclin A, anti-cyclin E were from Santa Cruz Biotechnology; anti-p-Histone H3(S10) from Millipore; anti-Grb14 (6).

Preparation of total RNA and gene expression analysis

Total RNA were extracted from mouse whole liver or from primary cultured hepatocytes using the SV Total RNA Isolation System (Promega). One µg was used for reverse transcription using Superscript II reverse transcriptase (Life Technologies) and (dT)15 primer and random primer (Promega). Quantitative real-time PCR (qRT-PCR) was performed using a SYBR Green PCR Master Mix (Roche Diagnostic). The data were expressed as relative mRNA and were normalized to 18S.

For human liver tissues, a preliminary RNA extraction step was performed using TRIzol Reagent (Life Technologies). Quantitative measurements of transcripts were performed by real-time PCR on a LightCycler 480 instrument (Roche) using SYBR Green chemistry and specific primers. For each sample, gene expression was normalized to that of HPRT mRNA content and was expressed relatively to the same calibrator. The relative quantity of each target gene was determined from replicate samples using the formula $2^{-\Delta\Delta Ct}$.

Transcriptomes preparation and data analysis

Gene expression profiles for liver from C57Bl/6 mice injected with recombinant adenovirus expressing scramble (USi, n=3) or Grb14 (Grb14i, n=3) shRNA were analyzed using Affymetrix Mouse Gene 1.0 ST arrays (Gene Expression Omnibus (GEO) dataset GSE81387). Samples were normalized using the RMA algorithm (Bioconductor *affy* package). Differential expression was measured with moderated t-test (limma R package). Gene set enrichment analyses (GSEA) (7) were performed with these data and with BioCarta and KEGG gene sets or with a dataset with invalidation of the three Rb genes in mice (TKO mice, GEO GSE19004 (8))

Immunohistochemistry

Liver tissue fragment fixed in 4% neutral buffered formalin overnight was embedded in paraffin and sectioned in 3 µm thick sections. Immunohistochemistry was performed with the anti-BrdU antibody (1/50, DakoCytomation) and revelation was performed using a secondary anti-mouse biotinylated antibody (1/500) and the Vectastain elite ABC kit (Vector Laboratories). Nuclei were counterstained with hematoxylin. To measure proliferation, we counted the frequency of BrdU-positive nuclei among 600 nuclei. TUNEL experiment was performed using *in situ* cell death detection kit (Roche) following manufacturer's instructions.

Statistical analysis

Results are reported as means +/- SEM. The comparison of different groups was carried out using Mann-Whitney test or one-way ANOVA. Differences were considered statistically significant at $p<0.05$.

REFERENCES

1. Guidotti JE, Bregerie O, Robert A, Debey P, Brechot C, Desdouets C. Liver cell polyploidization: a pivotal role for binuclear hepatocytes. J Biol Chem 2003;278:19095-19101.
2. Krek W, Livingston DM, Shirodkar S. Binding to DNA and the retinoblastoma gene product promoted by complex formation of different E2F family members. Science 1993;262:1557-1560.
3. Podevin P, Carpentier A, Pene V, Aoudjehane L, Carriere M, Zaidi S, Hernandez C, et al. Production of infectious hepatitis C virus in primary cultures of human adult hepatocytes. Gastroenterology 2010;139:1355-1364.
4. Blivet-Van Eggelpoel MJ, Chettouh H, Fartoux L, Aoudjehane L, Barbu V, Rey C, Priam S, et al. Epidermal growth factor receptor and HER-3 restrict cell response to sorafenib in hepatocellular carcinoma cells. J Hepatol 2012;57:108-115.
5. Nouaille S, Blanquart C, Zilberfarb V, Boute N, Perdereau D, Roix J, Burnol AF, et al. Interaction with Grb14 results in site-specific regulation of tyrosine phosphorylation of the insulin receptor. EMBO Rep 2006;7:512-518.
6. Kasus-Jacobi A, Perdereau D, Auzan C, Clauser E, Van Obberghen E, Mauvais-Jarvis F, Girard J, et al. Identification of the rat adapter Grb14 as an inhibitor of insulin actions. J. Biol. Chem. 1998;273:26026-26035.
7. Subramanian A, Tamayo P, Mootha VK, Mukherjee S, Ebert BL, Gillette MA, Paulovich A, et al. Gene set enrichment analysis: a knowledge-based approach for interpreting genome-wide expression profiles. Proc Natl Acad Sci U S A 2005;102:15545-15550.
8. Viatour P, Ehmer U, Saddic LA, Dorrell C, Andersen JB, Lin C, Zmoos AF, et al. Notch signaling inhibits hepatocellular carcinoma following inactivation of the RB pathway. J Exp Med 2011;208:1963-1976.

SUPPORTING DATA

Supporting Table S1 : Gene set enrichment analysis (GSEA) analysis of transcriptomic data from from C57Bl/6 mice injected with USi (n=3) or Grb14i (n=3) (GEO GSE81387) and with BioCarta and KEGG gene sets. See excel file.

Supporting Table S2: Clinicopathological characteristics of 85 patients with HCC

Age at diagnosis (years) Mean (± SD)	62.7 (± 12.3)
Sex ratio (M/F)	5.1 (71/14)
Etiology of chronic liver disease, n (%) HCV infection HBV infection Alcohol abuse Hemochromatosis NASH Combined viral hepatitis, metabolic syndrome and alcohol Undetermined	 21 (24.7) 27 (31.8) 5 (5.9) 2 (2.3) 11 (12.9) 13 (15.3) 8 (9.4)
Advanced fibrosis/cirrhosis, n (%)	49 (57.6)
Maximal tumour size, mean ± SD (mm)	65.2 ± 38.5
AFP (≥ 400 ng/ml), n (%)*	15 (17.6)
Multiplicity, n (%)	18 (21.2)
Tumour grade Well differentiated, n (%) Moderately differentiated, n (%) Poorly differentiated, n (%)	 21 (24.7) 41 (48.2) 23 (27)
CK19 expression, n (%)	17 (20)
Microvascular invasion, n (%)	40 (47)
Satellite nodules, n (%)	26 (30.5)

AFP: a-fetoprotein; CK19: cytokeratin 19; HCV: hepatitis C virus; HBV, hepatitis B virus; NASH, non alcoholic steatohepatitis
* four missing data

Supporting Table S3 : Relations between GRB14 mRNA fold inductions (T/NT) and the pathological characteristics of 85 HCC

	n	*GRB14 mRNA fold induction (T/NT)**	*P values*
HBV			
yes	27	0.80 [0.05 – 4.39]	0.336
no	58	0.66 [0.02 – 9.42]	
HCV			
yes	21	0.47 [0.10 – 2.31]	0.436
no	64	0.73 [0.02 – 9.42]	
NASH			
yes	11	0.41 [0.18– 6.50]	0.417
no	74	0.70 [0.02 – 9.42]	
MS + alcohol			
yes	8	0.77 [0.29 – 1.60]	0.503
no	77	0.68 [0.02 – 9.42]	
Alcohol			
yes	5	0.69 [0.23 – 1.06]	1.000
no	80	0.67 [0.02 – 9.42]	
Advanced fibrosis/cirrhosis			
yes	50	0.70 [0.05 – 4.39]	0.488
no	35	0.60 [0.02 – 9.42]	
AFP**			
< 400 ng/ml	47	0.70 [0.02 – 6.50]	0.681
≥ 400 ng/ml	34	0.65 [0.08 – 9.42]	
Tumour size			
< 5 cm	44	0.67 [0.05 – 6.50]	0.452
≥ 5cm	41	0.79 [0.02 – 9.42]	
Multiplicity			
yes	18	0.80 [0.08 – 9.42]	0.547
no	67	0.68 [0.02 – 6.50]	
Satellite nodules			
yes	26	0.68 [0.02 – 9.42]	0.347
no	59	0.66 [0.05 – 4.39]	
Differentiation			
well/moderate	61	0.78 [0.05 – 9.42]	**0.039**
poor	24	0.53 [0.02 – 1.68]	
CK19 expression			
< 5%	65	0.70 [0.05 – 6.50]	0.267
≥ 5%	17	0.52 [0.02 – 9.42]	
Microvascular invasion			
yes	41	0.63 [0.02 – 9.42]	0.358
no	44	0.74 [0.05– 6.50]	

AFP: a-fetoprotein; CK19: cytokeratin 19; HCV: hepatitis C virus;
HBV, hepatitis B virus; MS, metabolic syndrome; NASH, non alcoholic steatohepatitis

*Values are expressed as median [range]
** four missing data
** three missing data
All statistical analyses were performed using a Mann-Whitney test.

Supporting Figure S1 : C57Bl/6J mice injected with unspecific (USi) or Grb14 sh-adenovirus (Grb14i) were studied after 1 to 7 days (B-C), or after 2 days (A, D, E). (A) Phosphorylation levels of S6K on Thr389 and 4EBP1 on Ser65. Quantification of the ratio p-S6K/S6K and p-4EBP1/4EBP1 measured by Western blot is shown. Results are the mean ± SEM (n = 7-15 per group). *p<0.05 for Grb14i compared to USi mice. (B) Quantification of BrdU incorporation in USi or Grb14i liver sections (x20). (C) Western blot analysis of liver Grb14 expression. (D) TUNEL staining of liver sections (x20). (E) Plasma concentrations of alanine aminotransferase (ALAT) and aspartate aminotransferase (ASAT). Results are the mean ± SEM (n = 3-6 per group). ***p<0.005 for Grb14i compared to USi mice. For Western blot analysis, three representative samples are shown and GAPDH is used as loading control.

Supporting Figure S2 : (A) qRT-PCR analysis of IR-A and IR-B expression in liver from USi and Grb14i mice. Results are the mean ± SEM (n = 14-15 per group). ***p<0.005 for Grb14i compared to USi mice. (B) Semi-quantitative evaluation of IR isoforms expression in livers from USi and Grb14i mice. RT-PCR analysis was performed using a unique primer pair flanking exons 10 and 12 followed by analysis on 2% agarose gel.

Supporting Figure S3 : (A) Western blot analysis and scanning density quantification of Rb phosphorylation and expression in liver from WT and S6K DKO mice treated with USi or Grb14i. Results are the mean ± SEM (n = 3 to 4 per group). *p<0.05. (B) *e2f1* expression in WT and E2F1 KO littermate mice, treated with USi or Grb14i. Results are the mean ± SEM (n= 8 to 13 per group). ***p<0.005 for Grb14i compared to USi mice ; ### p<0.005 for E2F1 KO compared to WT mice.

Supporting Figure S4 : *GRB14* mRNA levels in human HCC and adjacent normal livers in data sets extracted from Oncomine (Roessler liver and Roessler liver 2 collections). Box and whisker plots showing median (horizontal line), interquartile range and min to max values of the data.

Supporting Figure S5 : IR status in human 85 paired HCC (T) and nontumoral adjacent liver parenchyma (NT). (A) IR-A expression. (B) Relative IR-A/IR-B ratio. IR-A and IR-B expression were quantified by qRT-PCR.

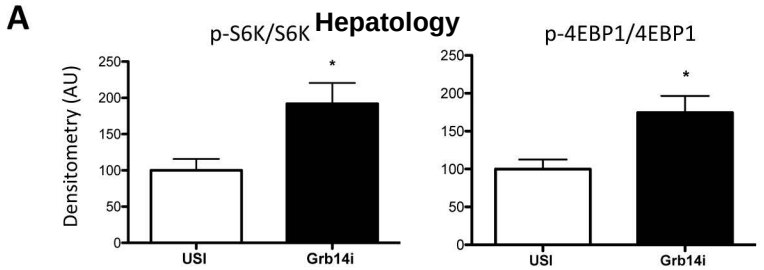

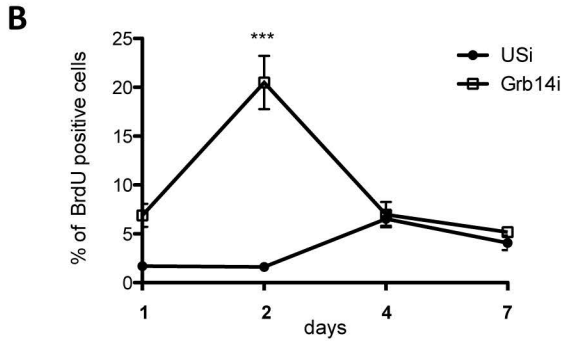

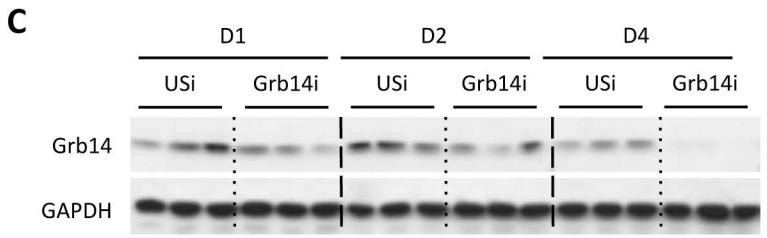

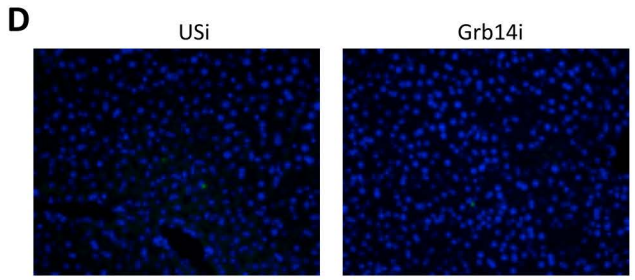

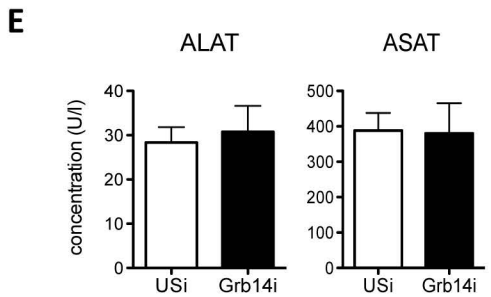

Supporting Figure S1

A

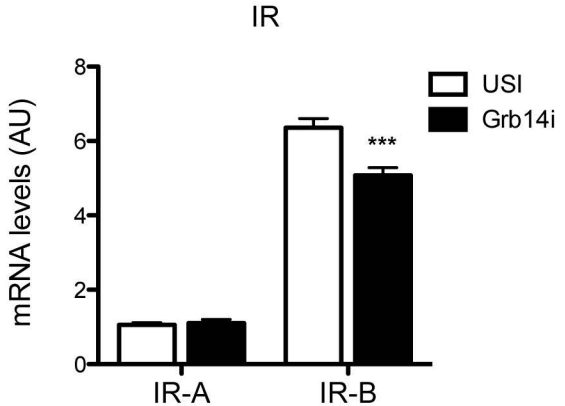

B

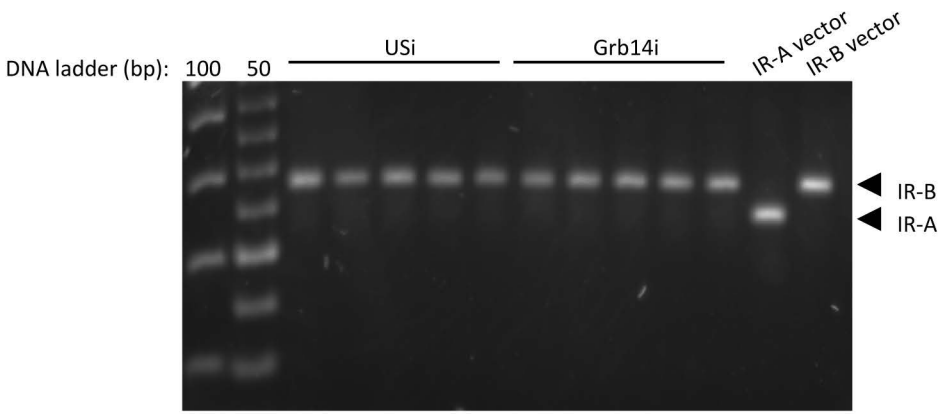

Supporting Figure S2

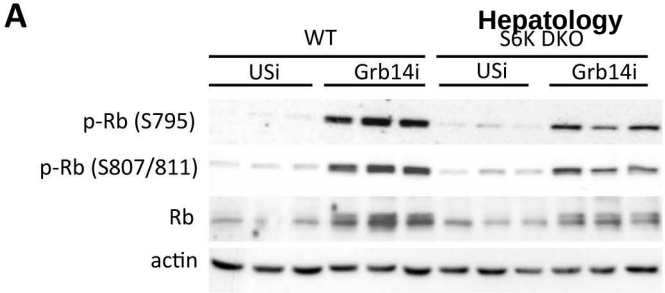

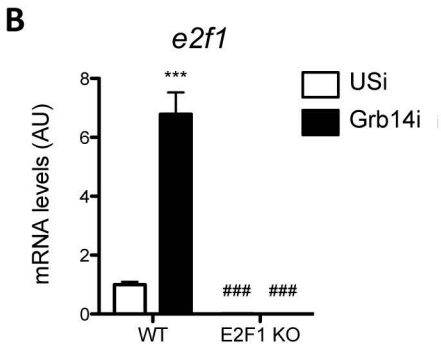

Supporting Figure S3

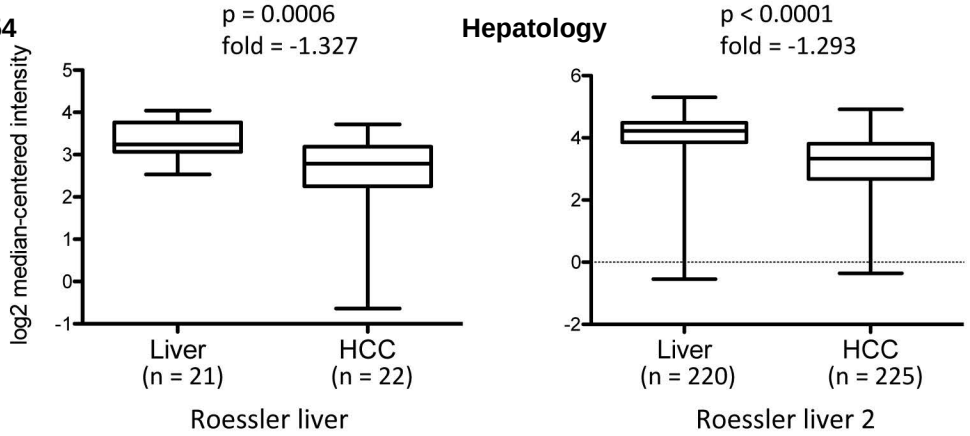

Supporting Figure S4

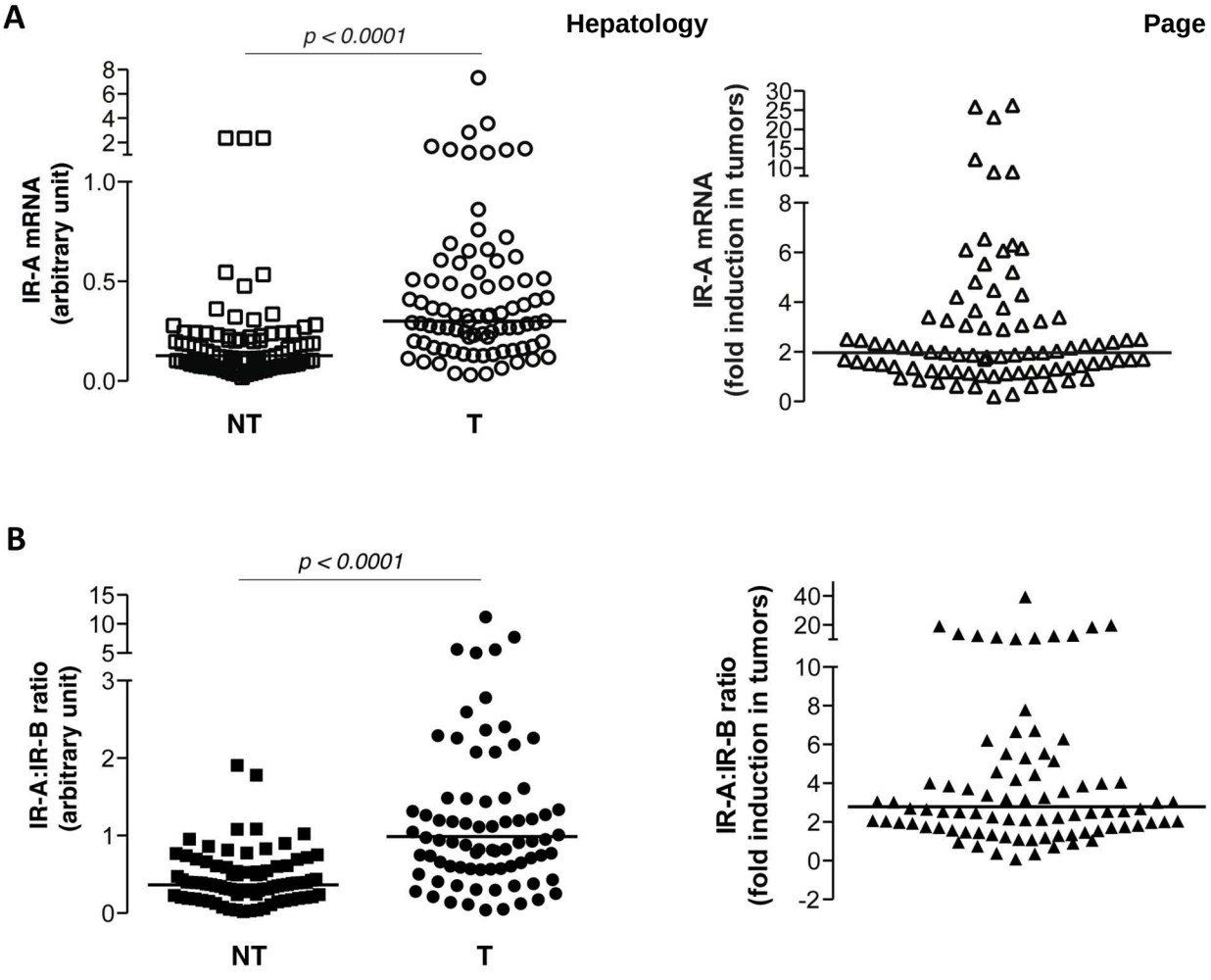

Supporting Figure 55

	NES	FDR.q.val
KEGG_CELL_CYCLE	2.7393727	0
KEGG_DNA_REPLICATION	2.6284354	0
BIOCARTA_MCM_PATHWAY	2.419913	0
KEGG_ABC_TRANSPORTERS	-2.3927069	0
BIOCARTA_G1_PATHWAY	2.3682327	0
BIOCARTA_G2_PATHWAY	2.3639038	0
KEGG_VALINE_LEUCINE_AND_ISOLEUCINE_DEGRADATION	-2.3625674	0
KEGG_OOCYTE_MEIOSIS	2.3205314	0
KEGG_HOMOLOGOUS_RECOMBINATION	2.2068677	0
BIOCARTA_ATRBRCA_PATHWAY	2.1728742	0
BIOCARTA_CELLCYCLE_PATHWAY	2.1548905	5.347594e-05
KEGG_MISMATCH_REPAIR	2.1064172	0.0003158068
KEGG_ARGININE_AND_PROLINE_METABOLISM	-2.106199	0.0025690398
BIOCARTA_LAIR_PATHWAY	-2.090894	0.0019267799
KEGG_PROGESTERONE_MEDIATED_OOCYTE_MATURATION	2.072623	0.0005706505
BIOCARTA_ATM_PATHWAY	2.065565	0.000560225
BIOCARTA_IL1R_PATHWAY	-2.0459363	0.0035320178
KEGG_CELL_ADHESION_MOLECULES_CAMS	-2.026559	0.0044942535
KEGG_REGULATION_OF_AUTOPHAGY	-2.016423	0.0041693607
KEGG_HEMATOPOIETIC_CELL_LINEAGE	-2.0053685	0.004660005
KEGG_HISTIDINE_METABOLISM	-2.0008242	0.004142227
KEGG_NUCLEOTIDE_EXCISION_REPAIR	2.000575	0.0012811087
BIOCARTA_IL12_PATHWAY	-1.9953915	0.004370867
BIOCARTA_IL2RB_PATHWAY	-1.9873655	0.0047034295
KEGG_P53_SIGNALING_PATHWAY	1.9619515	0.0017589286
KEGG_RIBOSOME	1.9583769	0.0016719697
BIOCARTA_IL7_PATHWAY	-1.94361	0.008743508
KEGG_PROPANOATE_METABOLISM	-1.9274518	0.010067887
KEGG_PYRIMIDINE_METABOLISM	1.9217632	0.0025464592
BIOCARTA_NO2IL12_PATHWAY	-1.9170498	0.011336976
KEGG_PROXIMAL_TUBULE_BICARBONATE_RECLAMATION	-1.9084638	0.0122752115
KEGG_ACUTE_MYELOID_LEUKEMIA	-1.9074398	0.011779058
KEGG_BASE_EXCISION_REPAIR	1.9035201	0.0033717614
KEGG_ALANINE_ASPARTATE_AND_GLUTAMATE_METABOLISM	-1.9003375	0.012171978
BIOCARTA_CSK_PATHWAY	-1.8977716	0.011828502
KEGG_T_CELL_RECEPTOR_SIGNALING_PATHWAY	-1.8935542	0.011414
KEGG_GLYCOLYSIS_GLUCONEOGENESIS	-1.89343	0.0108433
KEGG_DRUG_METABOLISM_CYTOCHROME_P450	-1.8914686	0.0107854325
KEGG_BUTANOATE_METABOLISM	-1.8816702	0.0121351415
KEGG_CYTOSOLIC_DNA_SENSING_PATHWAY	-1.8728565	0.012436132
KEGG_FATTY_ACID_METABOLISM	-1.8662852	0.01325583
KEGG_GLYCINE_SERINE_AND_THREONINE_METABOLISM	-1.8540395	0.014941905
KEGG_STEROID_BIOSYNTHESIS	-1.844601	0.015976567
KEGG_PEROXISOME	-1.8362898	0.01735792
KEGG_SPHINGOLIPID_METABOLISM	-1.8310623	0.01755542
KEGG_RETINOL_METABOLISM	-1.8262639	0.017601289
KEGG_COMPLEMENT_AND_COAGULATION_CASCADES	-1.8191103	0.018475236
KEGG_LYSOSOME	-1.8150942	0.018401872
KEGG_PRIMARY_IMMUNODEFICIENCY	-1.7996931	0.02051914
BIOCARTA_NFKB_PATHWAY	-1.7800556	0.025063049
KEGG_GRAFT_VERSUS_HOST_DISEASE	-1.7772573	0.02484496
KEGG_PYRUVATE_METABOLISM	-1.7733407	0.024749955
BIOCARTA_MYOSIN_PATHWAY	-1.763619	0.025954597
BIOCARTA_STRESS_PATHWAY	-1.7413101	0.031838737

KEGG_PRIMARY_BILE_ACID_BIOSYNTHESIS	-1.731619	0.03377933
BIOCARTA_RACCYCD_PATHWAY	1.7253594	0.025827767
KEGG_TRYPTOPHAN_METABOLISM	-1.723906	0.03583746
KEGG_SPLICEOSOME	1.6967795	0.033039436
KEGG_PPAR_SIGNALING_PATHWAY	-1.6917739	0.046074614
KEGG_NATURAL_KILLER_CELL_MEDIATED_CYTOTOXICITY	-1.6909338	0.045205444
KEGG_LEISHMANIA_INFECTION	-1.6898562	0.044458438
BIOCARTA_TOB1_PATHWAY	-1.6833404	0.045903627
BIOCARTA_PAR1_PATHWAY	-1.6735142	0.049400307
BIOCARTA_NTHI_PATHWAY	-1.6712672	0.049641296
KEGG_GLYCEROPHOSPHOLIPID_METABOLISM	-1.6689674	0.049574815
BIOCARTA_RELA_PATHWAY	-1.6638646	0.05025248
KEGG_PORPHYRIN_AND_CHLOROPHYLL_METABOLISM	-1.6629981	0.049459163
KEGG_GALACTOSE_METABOLISM	-1.648528	0.054744866
KEGG_GLYCOSPHINGOLIPID_BIOSYNTHESIS_GANGLIO_SERIES	-1.6421237	0.055885382
KEGG_BETA_ALANINE_METABOLISM	-1.6404983	0.055616397
KEGG_BASAL_CELL_CARCINOMA	-1.6354305	0.056874897
BIOCARTA_CTLA4_PATHWAY	-1.6294479	0.058296427
BIOCARTA_KERATINOCYTE_PATHWAY	-1.6256653	0.059049416
KEGG_PROTEIN_EXPORT	1.6246659	0.06056113
KEGG_LEUKOCYTE_TRANSENDOTHELIAL_MIGRATION	-1.6164666	0.06258658
KEGG_PHENYLALANINE_METABOLISM	-1.6138921	0.06263033
KEGG_FC_GAMMA_R_MEDIATED_PHAGOCYTOSIS	-1.6128892	0.06198277
KEGG_PANTOTHENATE_AND_COA_BIOSYNTHESIS	-1.6126622	0.06100964
KEGG_TOLL_LIKE_RECEPTOR_SIGNALING_PATHWAY	-1.6109443	0.060910758
KEGG_TYPE_I_DIABETES_MELLITUS	-1.6074289	0.06177825
KEGG_RIG_I_LIKE_RECEPTOR_SIGNALING_PATHWAY	-1.6067343	0.06116032
KEGG_RNA_DEGRADATION	1.6049858	0.06781889
KEGG_ONE_CARBON_POOL_BY_FOLATE	1.596521	0.06940514
KEGG_PRION_DISEASES	-1.5852203	0.07001306
KEGG_CHEMOKINE_SIGNALING_PATHWAY	-1.574331	0.074882515
KEGG_ETHER_LIPID_METABOLISM	-1.5730866	0.07460577
KEGG_VEGF_SIGNALING_PATHWAY	-1.571226	0.07440996
KEGG_B_CELL_RECEPTOR_SIGNALING_PATHWAY	-1.5637182	0.07758255
BIOCARTA_IL2_PATHWAY	-1.5527041	0.08274297
KEGG_CYTOKINE_CYTOKINE_RECEPTOR_INTERACTION	-1.5469459	0.08488286
KEGG_OTHER_GLYCAN_DEGRADATION	-1.5447026	0.085097544
KEGG_FC_EPSILON_RI_SIGNALING_PATHWAY	-1.5432744	0.08478853
BIOCARTA_ARAP_PATHWAY	-1.5402513	0.0855216
BIOCARTA_BARRESTIN_SRC_PATHWAY	-1.5346389	0.08717216
BIOCARTA_IL10_PATHWAY	-1.532537	0.08736009
KEGG_SYSTEMIC_LUPUS_ERYTHEMATOSUS	1.5255914	0.11786837
KEGG_INOSITOL_PHOSPHATE_METABOLISM	-1.5192238	0.09424031
BIOCARTA_NKCELLS_PATHWAY	-1.5109079	0.09724982
BIOCARTA_INTRINSIC_PATHWAY	-1.5100654	0.09664754
KEGG_BASAL_TRANSCRIPTION_FACTORS	1.5008394	0.13626873
BIOCARTA_AMI_PATHWAY	-1.4930143	0.10650163
BIOCARTA_HER2_PATHWAY	-1.4918332	0.10594526
BIOCARTA_P53HYPOXIA_PATHWAY	1.4843675	0.14756757
KEGG_NOTCH_SIGNALING_PATHWAY	-1.483031	0.11129629
KEGG_AMINO_SUGAR_AND_NUCLEOTIDE_SUGAR_METABOLISM	-1.4807603	0.11136016
KEGG_AXON_GUIDANCE	-1.4778264	0.112211026
KEGG_VASCULAR_SMOOTH_MUSCLE_CONTRACTION	-1.469734	0.11682697
BIOCARTA_GH_PATHWAY	-1.4688942	0.11616908
BIOCARTA_NKT_PATHWAY	-1.4677169	0.11559718
BIOCARTA_CXCR4_PATHWAY	-1.4657335	0.1155966
BIOCARTA_VEGF_PATHWAY	-1.4490018	0.12736045
KEGG_TYROSINE_METABOLISM	-1.4482245	0.12663507

KEGG_LINOLEIC_ACID_METABOLISM	-1.4386209	0.13313566
KEGG_REGULATION_OF_ACTIN_CYTOSKELETON	-1.4363984	0.13327993
KEGG_PURINE_METABOLISM	1.4304254	0.20556472
KEGG_ADIPOCYTOKINE_SIGNALING_PATHWAY	-1.4240769	0.14250064
BIOCARTA_ERK_PATHWAY	-1.420664	0.14372198
KEGG_NOD_LIKE_RECEPTOR_SIGNALING_PATHWAY	-1.415173	0.14634073
KEGG_MATURITY_ONSET_DIABETES_OF_THE_YOUNG	-1.4116176	0.14794144
BIOCARTA_HCMV_PATHWAY	-1.408836	0.14877634
KEGG_RNA_POLYMERASE	1.4082451	0.22774114
BIOCARTA_TOLL_PATHWAY	-1.407376	0.1484516
BIOCARTA_SPPA_PATHWAY	-1.4053646	0.1487124
BIOCARTA_GCR_PATHWAY	-1.3974007	0.154114
KEGG_EPITHELIAL_CELL_SIGNALING_IN_HELICOBACTER_PYLORI_INFECTION	-1.3890727	0.15993355
BIOCARTA_EDG1_PATHWAY	-1.3855525	0.16179492
KEGG_JAK_STAT_SIGNALING_PATHWAY	-1.379137	0.16584852
BIOCARTA_BIOPEPTIDES_PATHWAY	-1.3776872	0.16574012
BIOCARTA_RAC1_PATHWAY	-1.3753619	0.16621128
KEGG_SMALL_CELL_LUNG_CANCER	1.3685776	0.28068295
BIOCARTA_TCR_PATHWAY	-1.3620917	0.17693728
KEGG_FOCAL_ADHESION	-1.3505442	0.1870104
KEGG_NICOTINATE_AND_NICOTINAMIDE_METABOLISM	-1.3441538	0.19189493
KEGG_ENDOCYTOSIS	-1.3433124	0.19126455
KEGG_ALPHA_LINOLENIC_ACID_METABOLISM	-1.3421913	0.1905622
BIOCARTA_PROTEASOME_PATHWAY	1.3412738	0.31637028
KEGG_RENIN_ANGIOTENSIN_SYSTEM	-1.3389443	0.19228503
KEGG_GLYOXYLATE_AND_DICARBOXYLATE_METABOLISM	1.3251972	0.33441108
BIOCARTA_IL22BP_PATHWAY	-1.3244259	0.20533094
BIOCARTA_RHO_PATHWAY	-1.3210452	0.20732377
KEGG_PHOSPHATIDYLINOSITOL_SIGNALING_SYSTEM	-1.3198428	0.20667784
KEGG_NEUROACTIVE_LIGAND_RECEPTOR_INTERACTION	-1.306585	0.22006196
KEGG_FRUCTOSE_AND_MANNOSE_METABOLISM	-1.29017	0.23848586
BIOCARTA_CDC42RAC_PATHWAY	-1.276081	0.25398782
BIOCARTA_DC_PATHWAY	-1.2646002	0.26756856
BIOCARTA_TH1TH2_PATHWAY	-1.2617517	0.26898885
BIOCARTA_COMP_PATHWAY	-1.2411337	0.29568774
BIOCARTA_41BB_PATHWAY	-1.240763	0.29389146
KEGG_CYSTEINE_AND_METHIONINE_METABOLISM	-1.2396324	0.2931252
BIOCARTA_CHREBP2_PATHWAY	1.2387642	0.5080405
BIOCARTA_BCELLSURVIVAL_PATHWAY	1.2359923	0.4991284
BIOCARTA_MPR_PATHWAY	1.2353227	0.48550946
KEGG_INTESTINAL_IMMUNE_NETWORK_FOR_IGA_PRODUCTION	-1.2320892	0.30146405
KEGG_HEDGEHOG_SIGNALING_PATHWAY	-1.2310311	0.30080336
KEGG_GLYCEROLIPID_METABOLISM	-1.2275304	0.30396044
KEGG_STEROID_HORMONE_BIOSYNTHESIS	-1.2266266	0.30269223
BIOCARTA_AKT_PATHWAY	-1.2265527	0.3003098
BIOCARTA_MAPK_PATHWAY	-1.2211521	0.3057922
KEGG_GLYCOSAMINOGLYCAN_DEGRADATION	-1.211505	0.3183394
BIOCARTA_MAL_PATHWAY	-1.2106788	0.31728834
KEGG_TYPE_II_DIABETES_MELLITUS	-1.2099885	0.31600755
KEGG_MELANOGENESIS	-1.1994777	0.33020568
KEGG_PROSTATE_CANCER	1.1931632	0.57374656
KEGG_DORSO_VENTRAL_AXIS_FORMATION	1.1912282	0.561406
BIOCARTA_ECM_PATHWAY	-1.1881567	0.3456254
KEGG_ECM_RECEPTOR_INTERACTION	-1.1857022	0.3465727
KEGG_MAPK_SIGNALING_PATHWAY	-1.1829395	0.34830502
BIOCARTA_TNFR2_PATHWAY	-1.1814625	0.34792018
KEGG_BIOSYNTHESIS_OF_UNSATURATED_FATTY_ACIDS	-1.1762444	0.3535932
BIOCARTA_PTDINS_PATHWAY	-1.169315	0.36322388

KEGG_MELANOMA	-1.1611506	0.3744904
KEGG_AUTOIMMUNE_THYROID_DISEASE	-1.1465533	0.398126
KEGG_ALLOGRAFT_REJECTION	-1.1434119	0.40083832
BIOCARTA_SHH_PATHWAY	-1.1427759	0.39917487
KEGG_UBIQUITIN_MEDIATED_PROTEOLYSIS	1.1309364	0.7112896
BIOCARTA_TEL_PATHWAY	1.1290592	0.69743776
BIOCARTA_NO1_PATHWAY	-1.1260861	0.42753482
KEGG_SELENOAMINO_ACID_METABOLISM	-1.1190732	0.4374933
BIOCARTA_ARF_PATHWAY	1.1177137	0.7111043
BIOCARTA_STATHMIN_PATHWAY	-1.1164043	0.4392375
BIOCARTA_MET_PATHWAY	-1.1127336	0.44286773
BIOCARTA_CARDIACEGF_PATHWAY	-1.1112835	0.4423766
BIOCARTA_IL6_PATHWAY	-1.110977	0.44000086
KEGG_METABOLISM_OF_XENOBIOTICS_BY_CYTOCHROME_P450	-1.1024216	0.45397952
BIOCARTA_CCR3_PATHWAY	-1.0991234	0.4573714
KEGG_PANCREATIC_CANCER	1.0973718	0.75117177
BIOCARTA_ETS_PATHWAY	1.0946121	0.7404559
KEGG_AMYOTROPHIC_LATERAL_SCLEROSIS_ALS	-1.0888096	0.4747365
KEGG_GAP_JUNCTION	1.0870419	0.74359846
BIOCARTA_TPO_PATHWAY	-1.0865775	0.47637257
BIOCARTA_CD40_PATHWAY	-1.0824887	0.4810396
KEGG_CARDIAC_MUSCLE_CONTRACTION	1.0818914	0.7402093
KEGG_GLUTATHIONE_METABOLISM	1.0768974	0.7367232
BIOCARTA_PDGF_PATHWAY	-1.0708735	0.501855
KEGG_RIBOFLAVIN_METABOLISM	-1.0699977	0.50031734
BIOCARTA_ACH_PATHWAY	-1.0545992	0.529016
KEGG_INSULIN_SIGNALING_PATHWAY	-1.0487655	0.53855234
BIOCARTA_FAS_PATHWAY	1.0476384	0.7999242
BIOCARTA_PGC1A_PATHWAY	1.0369705	0.8119731
BIOCARTA_HIF_PATHWAY	-1.0328934	0.56936646
KEGG_CALCIUM_SIGNALING_PATHWAY	-1.0253541	0.58227557
BIOCARTA_FMLP_PATHWAY	-1.0247566	0.58013254
KEGG_TGF_BETA_SIGNALING_PATHWAY	-1.0246607	0.576707
KEGG_COLORECTAL_CANCER	1.0228635	0.8335131
BIOCARTA_MITOCHONDRIA_PATHWAY	1.0201031	0.8234814
KEGG_APOPTOSIS	-1.0178387	0.58767456
BIOCARTA_FCER1_PATHWAY	-1.0021625	0.6200977
BIOCARTA_INFLAM_PATHWAY	0.9914221	0.8868759
BIOCARTA_CYTOKINE_PATHWAY	-0.99113804	0.6427485
KEGG_GLYCOSYLPHOSPHATIDYLINOSITOL_GPI_ANCHOR_BIOSYNTHESIS	-0.9895248	0.6426254
KEGG_STARCH_AND_SUCROSE_METABOLISM	-0.9893538	0.6390864
KEGG_ANTIGEN_PROCESSING_AND_PRESENTATION	-0.98718536	0.6400621
BIOCARTA_ALK_PATHWAY	-0.9828504	0.6461438
BIOCARTA_IGF1_PATHWAY	-0.9794809	0.6498568
BIOCARTA_IGF1MTOR_PATHWAY	0.9769246	0.90934175
KEGG_TASTE_TRANSDUCTION	0.97497576	0.8963154
KEGG_THYROID_CANCER	-0.97407395	0.65870047
KEGG_NON_SMALL_CELL_LUNG_CANCER	-0.96681845	0.6721487
KEGG_LONG_TERM_DEPRESSION	-0.9511978	0.7047854
KEGG_ARACHIDONIC_ACID_METABOLISM	-0.94568557	0.71419364
KEGG_DRUG_METABOLISM_OTHER_ENZYMES	0.94418705	0.963425
KEGG_PENTOSE_PHOSPHATE_PATHWAY	-0.9429845	0.716295
KEGG_ERBB_SIGNALING_PATHWAY	-0.9383427	0.7230868
BIOCARTA_SPRY_PATHWAY	-0.93293	0.73111326
KEGG_HUNTINGTONS_DISEASE	0.9328009	0.9752295
KEGG_N_GLYCAN_BIOSYNTHESIS	0.9300227	0.9639633
KEGG_VASOPRESSIN_REGULATED_WATER_REABSORPTION	-0.92720383	0.74057114
KEGG_ENDOMETRIAL_CANCER	-0.92507607	0.741166

BIOCARTA_TID_PATHWAY	-0.9214274	0.7453602	
BIOCARTA_GLEEVEC_PATHWAY	-0.9202868	0.7437639	
BIOCARTA_INSULIN_PATHWAY	-0.9021251	0.7809233	
KEGG_LYSINE_DEGRADATION	-0.898462	0.78475714	
BIOCARTA_CDMAC_PATHWAY	-0.8983203	0.78075856	
BIOCARTA_PPARA_PATHWAY	0.87663275		1
KEGG_ADHERENS_JUNCTION	-0.87148243	0.83573925	
BIOCARTA_EGF_PATHWAY	-0.86952966	0.835297	
KEGG_BLADDER_CANCER	0.86902344		1
KEGG_PATHWAYS_IN_CANCER	0.862868		1
KEGG_WNT_SIGNALING_PATHWAY	-0.8615491	0.84700733	
KEGG_GLIOMA	0.860394		1
KEGG_GLYCOSAMINOGLYCAN_BIOSYNTHESIS_CHONDROITIN_SULFATE	-0.85661364	0.85253155	
BIOCARTA_EIF4_PATHWAY	-0.8474534	0.86652565	
BIOCARTA_CK1_PATHWAY	-0.8404916	0.8754715	
BIOCARTA_CALCINEURIN_PATHWAY	0.8281449		1
KEGG_GNRH_SIGNALING_PATHWAY	-0.82002115	0.9098307	
KEGG_RENAL_CELL_CARCINOMA	-0.8086713	0.92594695	
BIOCARTA_MTOR_PATHWAY	0.8077915		1
BIOCARTA_BAD_PATHWAY	0.8032015		1
BIOCARTA_CTCF_PATHWAY	-0.7870396	0.9580654	
KEGG_ASTHMA	-0.78573745	0.95520914	
KEGG_PATHOGENIC_ESCHERICHIA_COLI_INFECTION	-0.78565675	0.95033115	
BIOCARTA_BCR_PATHWAY	-0.7801709	0.9542938	
BIOCARTA_CASPASE_PATHWAY	-0.77817005	0.95256007	
BIOCARTA_AT1R_PATHWAY	-0.7773184	0.9489741	
KEGG_MTOR_SIGNALING_PATHWAY	0.7758864		1
BIOCARTA_IGF1R_PATHWAY	0.76383954		1
KEGG_VIRAL_MYOCARDITIS	0.75624263		1
BIOCARTA_NFAT_PATHWAY	0.752076		1
KEGG_PROTEASOME	0.7511516		1
KEGG_ALDOSTERONE_REGULATED_SODIUM_REABSORPTION	0.7505752		1
KEGG_O_GLYCAN_BIOSYNTHESIS	0.74268		1
BIOCARTA_P38MAPK_PATHWAY	-0.7351197		1
BIOCARTA_AGR_PATHWAY	-0.7263676		1
BIOCARTA_VIP_PATHWAY	-0.7239398		1
KEGG_OXIDATIVE_PHOSPHORYLATION	0.7228392		1
KEGG_ALZHEIMERS_DISEASE	-0.7222655		1
KEGG_GLYCOSAMINOGLYCAN_BIOSYNTHESIS_HEPARAN_SULFATE	0.7222216		1
KEGG_CITRATE_CYCLE_TCA_CYCLE	-0.71837944		1
BIOCARTA_RAS_PATHWAY	-0.71357554		1
BIOCARTA_GPCR_PATHWAY	-0.7007401		1
BIOCARTA_IL3_PATHWAY	-0.6944882		1
KEGG_OLFACTORY_TRANSDUCTION	0.6930238		1
KEGG_ARRHYTHMOGENIC_RIGHT_VENTRICULAR_CARDIOMYOPATHY_ARVC	-0.69172525		1
BIOCARTA_PYK2_PATHWAY	-0.6848684		1
BIOCARTA_WNT_PATHWAY	0.6848396		1
BIOCARTA_DEATH_PATHWAY	-0.677364		1
BIOCARTA_TFF_PATHWAY	-0.6764886		1
BIOCARTA_HIVNEF_PATHWAY	-0.67072845		1
KEGG_GLYCOSPHINGOLIPID_BIOSYNTHESIS_LACTO_AND_NEOLACTO_SERIES	-0.66950035		1
KEGG_PARKINSONS_DISEASE	-0.6689508	0.99620813	
BIOCARTA_MCALPAIN_PATHWAY	-0.6623327	0.9960744	
KEGG_NEUROTROPHIN_SIGNALING_PATHWAY	-0.6603868	0.9925571	
BIOCARTA_GATA3_PATHWAY	0.65777916		1
BIOCARTA_UCALPAIN_PATHWAY	0.65528196		1
KEGG_HYPERTROPHIC_CARDIOMYOPATHY_HCM	0.6552235		1
BIOCARTA_NGF_PATHWAY	-0.65180737	0.9932271	

KEGG_CHRONIC_MYELOID_LEUKEMIA	0.65102535		1
BIOCARTA_PTEN_PATHWAY	0.6452016		1
BIOCARTA_INTEGRIN_PATHWAY	-0.6437791	0.99339247	
KEGG_AMINOACYL_TRNA_BIOSYNTHESIS	0.6435553		1
KEGG_DILATED_CARDIOMYOPATHY	0.64302194		1
BIOCARTA_TNFR1_PATHWAY	0.63777196		1
BIOCARTA_PML_PATHWAY	-0.6208486		1
KEGG_SNARE_INTERACTIONS_IN_VESICULAR_TRANSPORT	-0.6197577	0.99652267	
BIOCARTA_EPO_PATHWAY	-0.615938	0.99364007	
BIOCARTA_ERK5_PATHWAY	-0.6118367	0.9908755	
KEGG_TIGHT_JUNCTION	0.61105794		1
BIOCARTA_CREB_PATHWAY	0.61045784		1
BIOCARTA_CARM_ER_PATHWAY	0.6094333		1
BIOCARTA_GSK3_PATHWAY	-0.5999915	0.9908751	
BIOCARTA_MEF2D_PATHWAY	0.58659357		1
KEGG_LONG_TERM_POTENTIATION	0.5798464		1
BIOCARTA_HDAC_PATHWAY	0.5778936		1
KEGG_VIBRIO_CHOLERAE_INFECTION	-0.56353146	0.99762285	
BIOCARTA_NOS1_PATHWAY	0.5572001		1
BIOCARTA_CHEMICAL_PATHWAY	0.5559863		1
BIOCARTA_RARRXR_PATHWAY	-0.50921345		1
BIOCARTA_NDKDYNAMIN_PATHWAY	0.49697408		1
BIOCARTA_ACTINY_PATHWAY	0.49516785		1
BIOCARTA_CERAMIDE_PATHWAY	-0.457886		1
BIOCARTA_CCR5_PATHWAY	0.428468	0.9984397	
BIOCARTA_TGFB_PATHWAY	-0.41669756	0.99932027	